POLITECNICO
DI TORINO

Department of Applied Science and Technology

Master Thesis in Nanotechnologies for ICT's

Radio-Sensitization of Gold Nanoparticles *In Ovo* and *In Vivo* as a Therapeutic for Lung Cancer

Supervisors:

Prof. Matteo Cocuzza

Prof. Carly Filgueira

Prof. Alessandro Grattoni

Candidate:

Veronica Vighetto

July 2018

A mamma e papa`,

And then while I'm away
I'll write home every day
And I'll send all my loving to you.

-All my lovings, The Beatles

Abstract

Cancer is a major public health problem worldwide and is the second leading cause of death in the United States. Approximately 50% of all cancer patients receive radiation as a treatment. Surrounding normal tissues are also affected by the radiation, which cannot distinguish between healthy and cancer cells. As a result, the general dose of radiation administered must be limited in order to keep normal tissue toxicities at a tolerable level.

For this reason, the use of radioenhancers has been investigated as one approach to lower the general delivered radiation dose and, in particular, gold nanoparticles (GNPs) have been the main candidates for this purpose due to the fact that they are inert biocompatible materials with very low toxicity. This thesis focuses on the demonstration of the radioenhancement capabilities of unfunctionalized GNPs on Lewis lung (Luciferase expressing) cell-derived tumors. The work evolves from *in vitro* to *in vivo* experiments, and a new alternative model is presented: the chick chorioallantoic membrane (CAM). Being immunodeficient, fecundated chicken eggs can host, on their CAM, any type of cells, resulting in an ideal environment for tumor growth due to the presence of a blood vessel network that can aliment the carcinoma. To validate the results of the *in ovo* experiments, similar experiments were performed *in vivo* with C57/BL6 mice. This work verifies that the CAM is a robust and efficient model to obtain preliminary data on the synergistic effect of gold nanoparticles and x-ray radiation. This particular research will translate to lower radiation doses required in the clinic, improving patient outcomes through less invasive treatment, faster recovery, and reduced damage to healthy tissue.

Acknowledgments

I would like to thank all of the Grattoni lab and the department of Nanomedicine of the Houston Methodist Research Institute. Special thanks go to Prof. Alessandro Grattoni, which gave me the opportunity to join the lab and help me with my future, and to Prof. Carly Filgueira, who is the most kind and patient mentor possible and is a great teacher, and a passionate scientist and I'm esteemed to have the possibility to learn from her and work with her.

Thanks to Fer for all the laughs and for teaching me how to dance in a Mexican wedding, you are amazing! Thanks also to Antonia, Jessica, and Corrine (even if you are super bossy, also with your boss) for helping me and teaching me a lot of cool mouse and lab work. Thanks to Giacomo, the bomber Farina, Giovanni, Antons, Jeremy, and Antonia because you guys are part of this incredible and unforgettable experience. Thanks to the Italian group of IMT: Francesca, Nico Afro, Nicola, Matteo (future Noble prize) and Maria Luisa (sei sempre più bella e brava tu) for all the afternoons, evenings, and trips spent together, you made me feel at home. Thanks to Sid for all of the experiences lived together and for helping Maria and I in a lot of occasions.

And the last, but absolutely not the least, thanks go to Maria, my roommate. I was so lucky to meet you, you were my family for 8 months! Thanks for all the laughs, thanks for all the special moments spent at home, thanks for all the discussion and conversation, and thanks for the best trip ever in my live. I will miss you a lot!

Questa tesi è la conclusione di 8 mesi di lavoro negli Stati Uniti, che sono stati bellissimi e durissimi insieme. Anche se a migliaia di km di distanza ho ricevuto il supporto dei miei amici più cari, che hanno ascoltato le mie paranoie, le mie paure e i miei sfoghi, e mi siete mancati tanto.

Quindi voglio ringraziare Giulia, Lela e Lonni, voi siete le mie rocce, grazie di esserci state e di esserci sempre da tanti anni, non sarei la stessa senza di voi. Grazie a Antimi, che mi ha addirittura abbracciato quanto sono tornata a casa!!, perché mi hai dimostrato che la nostra amicizia è un punto fisso, non importa dove siamo nel mondo (ma meglio se siamo nello stesso stato). Grazie a Kekka e a Simona e Lucrezia perchè nonostante tutte le novità, noi siamo ancora qui. Grazie a Badiali, perché ti sei sorbito i miei discorsi su cosa scegliere per il mio futuro e per esserci sempre, perché io e te abbiamo lo stesso carattere e anche se insieme siamo noiosi, ci vogliamo bene. Grazie a Beneduce e Niccolò per la stupidità, le risate, i sorrisi che mi avete fatto vivere anche mentre ero lontana, molto spesso sono serviti per tirarmi su il morale in momenti di sconforto. E un grazie va anche a Simone e Marco per lo studio insieme, il divertimento e le discussioni e soprattutto per il supporto durante questa magistrale. Infine, il grazie più grande e più profondo va a mia Mamma e mio Papà perché mi hanno permesso di vivere questa esperienza, perché mi hanno cresciuta ed educata, e sono contenta e orgogliosa che siano i miei genitori.

Content

Chapter 1

Introduction

1.1 Cancer and Radiotherapy

Cancer is a major public health problem worldwide and is the second leading cause of death in the United States[1]. The most common causes of cancer death are cancers of the lung, prostate, and colorectum in men and the lung, breast, and colorectum in women. These four cancers account for 45% of all cancer deaths, with one-quarter due to lung cancer.[1] The National Institutes of Health estimated that in 2017 the overall cost for the cancer care was $147.3 billion dollars, $13.9 billion dollar of which was due to lung cancer[2].

Depending on the stage and type of tumor different treatment modalities are available, such as radiation therapy, surgery, chemotherapy, immunotherapy and hormonal therapy or a combination of them. Radiation therapy remains an important component of cancer treatment with approximately 50% of all cancer patients receiving radiation therapy during their course of illness[34].

The aim of radiation therapy is to exploit the effect of ionizing radiation to destroy cancer cells. Electrically charged particles deposit their energy in the cells of the tissue, causing genetic damages, resulting in cell death. Exposure to high-energy radiation causes direct or indirect ionization of the atoms which make up the DNA chain. Although cells have mechanisms for repairing single-strand DNA damage and double-stranded DNA damage, the double-stranded DNA breaks are much more difficult to repair and can lead to dramatic chromosomal abnormalities and genetic deletions. These lesions can block genome replication and transcription, blocking their ability to divide and proliferate further[5].

To deliver radiation to the tumor area two ways can be exploited. Internal radiation or

brachytherapy is delivered directly inside the body by radioactive sources, seeds directly into the tumor sit. This strategy is particularly used in routine treatment based on its short range effects[3]. External beam radiation is delivered from outside the body by aiming high-energy rays (photons, protons or particle radiation) to the location of the tumor, making this the most common approach in a clinical setting[3].

One of the major challenges of radiotherapy is its lack of selectivity due to the similar mass energy absorption properties of both cancer and healthy tissues[6]. This is the reason why a current goal of radiation therapy is to maximize the radiation dose to abnormal cancer cells while minimizing exposure to normal cells, which are adjacent to cancer cells or in the path of radiation[3].

In order to achieve this goal, agents have been found to improve the contrast between the tumor and soft tissues, presenting radiosensitizing properties, that allow for an overall lower exposure dose, potentially improving tumor control, reducing side effects and increasing survival when compared to radiotherapy alone[6].

1.2 Radiosensitization and Nanotechnology

Exposure to Ionizing Radiation (IR) effectively achieves tumor control but can also affect the surrounding healthy tissue. Over the past decades, considerable improvements have been made in order to increase the precision and the accuracy of radiation delivery. Technological innovations which combine the intensity modulation of radiation and image guiding[7] have been investigated to increase precision in the delivery of radiation. Additionally, personalized treatment approaches, which require the development of a larger arsenal of agents acting on molecular pathways involved in radiation response and utilize targeted drugs, are under investigation[8].

Nanotechnology has also emerged as a promising strategy to enhance radiotherapeutic effects. Nanoparticle technology exploits the development of a new generation of cancer therapies, capable to overcome many biological and biophysical barriers, increasing the effectiveness with respect standard radiotherapy and intervention. Nanoparticles can selectively gain the access to tumor due to their small size and modifiability, providing better penetration of therapeutic and diagnostic substances within the body at a reduced risk when compared to conventional cancer therapy[9].

Nanoparticles can effectively target a tumor by exploiting the Enhanced Permeability and Retention (EPR) effect. This preferential accumulation of nanoparticles in the tumor region can be

used for several different purposes: to improve contrast enhancement for imaging, to specifically delivery chemotherapeutic agents, or to locally increase a dose of radiation[10].
Multi-disciplinary research performed over the past decade has demonstrated the potential of gold nanoparticles application in preclinical studies, which can be successfully translated into clinical practice.
Gold nanoparticles (GNPs) offer a means to transport agents to diseased cells or tissues in combination with unique size-dependent physio-chemical and optical properties, adaptability, sub-cellular size, and biocompatibility[11]. They can be involved for both cancer therapeutics and diagnostic and have been demonstrated as novel contrast agents for molecular imaging, computed tomography (CT) imaging, and photothermal cancer therapy[1213]. The high atomic number of elemental gold (Z=79) compared to that of soft tissues, permits metal enhanced radiotherapy, where the presence of GNPs can amplify delivered ionizing radiation. Therefore, GNPs can be used to deliver a significantly greater amount of energy per unit mass at a tumor site, increasing the local dose of radiation deposited[10].

1.3 Research Objectives

The objective of this study is to demonstrate the use of gold nanoparticles as radiosensitizers in the treatment of lung cancer. The idea is to exploit gold nanoparticles of two different sizes to analyze their effectiveness using a Lewis lung (Luciferase expressing) cell line, highly tumorigenic for C57/BL6 mice. This work evolves from *in vitro* tests to *in vivo* analysis, exploiting two different animal models: the chick chorioallantoic membrane (CAM), also referred to as an *in ovo* system, which generates an ideal environment for tumor growth due to the presence of a blood vessel network that can aliment the carcinoma, and the more standard mouse model, using C57/BL6 mice.

Chapter 2

Mechanisms of Action

2.1 Introduction

Gold Nanoparticles (GNP) are defined as particles with diameter between ~1 nm and ~100 nm. One of the major advantage of this technology is the synthetic versatility, which enables tailoring of particle size, shape and surface properties. The variation of these parameters permits synthesis of GNPs with different and unique chemical, optical and electronic properties, which can be exploited for various biomedical applications.

The optical and electronic properties of GNPs make them an excellent absorber of X-ray for medical application: the high atomic number of elemental gold (Z=79) compared to that of soft tissues permits metal enhanced radiotherapy, where the presence of GNPs can amplify delivered ionizing radiation. Therefore, GNPs can be used to deliver a significantly greater amount of energy per unit mass at a tumor site, increasing the local dose of radiation deposited[10].

Current theory suggests that gold nanoparticle-mediated radiosensitization is a combination of physical, chemical, and biological effects, as shown in Fig. 1.

In the following section these mechanisms will be discussed considering three different phases of radiation effect on biological system.

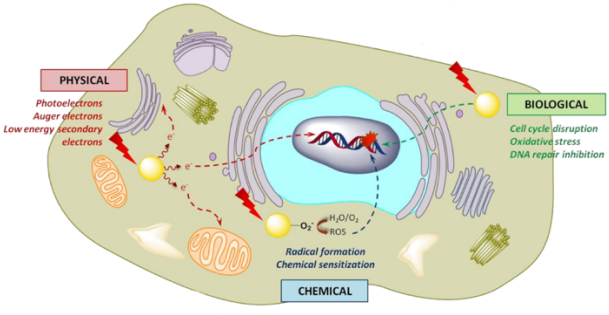

Figure 1. Mechanisms of GNP radiosensitization

2.2 Physical enhancement

The physical phase is the first one that occurs nanoseconds after IR exposure. The radiation interacts with biomolecules to cause ionization or excitation, generating free radicals.
Two of the main competitive mechanisms of energy absorption that lead to cellular damages by increasing the number of free electrons include: the Compton effect and photoelectric effect.
Compton effect is the primary mechanism by which electrons can lose energy in soft tissue[6].
An energetic photon is scattered by a weakly bound electron and a transfer of energy between the photon and the electron occurs, typically leading to the ejection of the electron from the atom (Fig. 2a). In this case photons tend to retain the majority of their energy after the collision, so they have a longer range of collision leading to very sparse distribution of ionizing events.

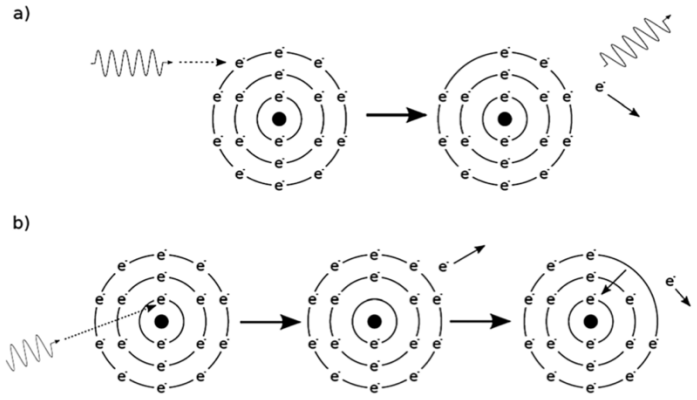

Figure 2. Schematic illustration of ionizations caused by (a) Compton and (b) photoelectric effect

In the photoelectric effect, shown in Fig. 2b, an incident photon is absorbed by an atom-bound electron leading to the ejection of an inner-shell electron (ionizing event). The outer-shell electrons fall to fill the vacancy (relaxation event), causing the release of low energy photons (fluorescence) and cascade of Auger electrons.
As opposed to the Compton effect, in this case the absorption of the photon can only occur in the presence of an atomic nucleus to allow for the conservation of momentum. Due to the nature of the

photoelectric effect, this mechanism is strongly dependent on the photon energy as well as the binding energy of the electron. As a result, the cross-section of the photoelectric effect, which refers to the probability of a material interacting with the radiation, depends on the atomic number of the atom, scaling as roughly as Z^4. By exploiting the atomic number difference between gold and soft tissues, which are primarily composed of organic material with low atomic numbers, GNPs can be used to deliver a significantly greater amount of energy per unit mass, increasing the local dose of radiation deposited in the tumor.

2.3 Chemical enhancement

The chemical phase of radiation exposure involves two possible mechanisms, according to the cellular localization of GNPs.

The first mechanism requires nuclear localization of GNPs to cause the chemical sensitization of DNA leading to irradiation damages. Low energy electrons do not produce considerable secondary electrons upon interaction with GNPs: for example the emitted Auger electrons do not have enough energy to ionize again other atoms, but it is demonstrated that they can cause the greatest DNA damage[10]. Low energy electrons cause the formation of transient negative ions, which increase the sensitivity of DNA to fragmentation and considerable increase the probability of damaging DNA[14].

With the second mechanism, the radical formation and catalysis is increased due to the activation of the GNP surface. The small size and the high curvature of the nanoparticles modify the highly organized structure of bulk gold, causing an alteration of the electronic configuration of surface atoms, enabling radical production at the reactive surface of GNPs. In this way, the surface of the GNPs is electronically active and capable of catalyzing chemical reactions. Small particles with large surface area can transfer electrons from surface-bond donor groups to O_2 to generate superoxide radicals, enhancing the reactive ion species (ROS) production. The ROS production causes cellular damage including oxidation of lipids, proteins, and DNA, resulting in apoptotic and necrotic cell death due to mitochondrial dysfunction[6].

2.4 Biological enhancement

The biological phase is the last one that occurs, and it enhance the effects of IR via oxidative stress, cell cycle disruption and DNA repair inhibition.

One of the primary pathways of radiation-induced cell killing is the radiolysis of water, generating free radicals and ROS, that interact with various cellular component leading to oxidative stress and triggering cell death via apoptosis or necrosis. As discussed before (section 1.3 of chapter 2) GNPs induce the formation of ROS. Although studies have been performed in support of GNP- induction of ROS[15][16], the precise mechanism leading to the biological enhancement of radiation effects remains to be clarified.

The major biological component of cell sensitivity to radiation is the cell cycle: cells display different radiation sensitivity during different phases of the cell cycle. The irradiation exposure causes a delay in the movement of the cells through the different cycle phases, which is one of the main pathways of DNA damage. It has been demonstrated that GNPs cause cell cycle disruption[17]. The effect is dependent on various factor, including physio-chemical characteristics.

Slowing the progression of the cells through the cell cycle cannot be sufficient: cells naturally maintain genomic integrity by repairing radiation-induced damages, in case of unsuccess the activation of the cell death event occurs. GNPs can enhance the pathways responsible for the DNA repair inhibition.

Chapter 3

Material and methods

3.1 Gold Nanoparticles

Two different sizes of gold nanoparticle are synthesized: one batch of particles has an expected diameter dimension of ~ 4 nm (called Small Gold Nanoparticles, SGNPs), the other batch of particles has an expected diameter of ~ 37 nm (called Big Gold Nanoparticles, BGNPs). Both sizes of particles are tested to investigate the radiosensitivity effects.
To create these two type of particles, two different synthesis methods are used. SGNPs and BGNPs are characterized using the same analytical techniques and instruments.

3.1.1 Synthesis

SGNP

Small GNPs (SGNPs) were synthesized according to Duff et al.18 using Tetrakis(hydroxymethyl)phosphonium chloride (Sigma-Aldrich, 404861) and Hydrogen tetrachloroaurate(III) hydrate (Sigma-Aldrich, 254169).
Briefly, a solution with 1.2 ml 1N NaOH in 120 ml of Milli-Q water is prepared. In another beaker a solution of 33 ml of MilliQ water with 400 µl of THPC (tetrakis-hydroxymethyl- phosphonium chloride) is made. 4 ml of this solution are added to the NaOH one and let it stir for 5 minutes at a speed of 400 rpm. Finally, 6.75 ml of aged (at least 3 days) 1% chloroauric acid is quickly poured in the stirring beaker. For this last step high stirring speed is required to create only one nucleation center, in order to obtain the particles as monodisperse as possible. The resulting size is very small

(few nanometers), but the sample has to be stored for at least two weeks at 4 °C. During this period of time particle ripening will occur, increasing the particle diameter up to ~4 nm.

BGNP

Big GNPs (BGNP) were synthesized using citric acid (Sigma, C3674) and Gold (III) Chloride (Sigma, 379948).

Briefly, 600 ul of MilliQ was added to an Erlenmeyer flask and placed on a hot plate until vigorous boiling. After 30s of refluxing, 4.8 ml of 0.039 M aqueous citrate was added to the flask. Finally, after about one minute, 7 ml of 0.033 M Gold (III) Chloride was rapidly added to the boiling solution and left on the hot plate for four minutes until the observed color change, from a dark gray to yellowish and again to red, was complete. The solution is allowed to cool and stored at room temperature. To concentrate the nanoparticle solution the centrifugation method is used.

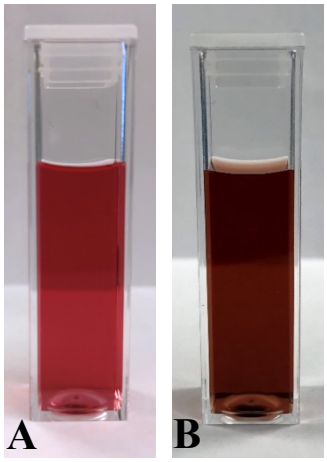

Figure 3. Optical image of (A) SGNP and (B) BGNP

3.1.2 Characterization

The size of the particles is measured using Dynamic Light Scattering (DLS), Scanning Electron Microscopy (SEM), Atomic Force Microscopy (AFM) and Transmission Electron Microscopy (TEM). Z-potential and absorbance spectra are also measured, the absorbance spectra measurements are performed using UltraViolet-visible spectrometer (UV-vis). Concentration analysis are performed using the UV-vis spectrometer and the results are supported by Inductively Coupled Plasma Mass Spectrometer (ICP-MS) measurements.

DLS

Dynamic light scattering is an optical technique used for analyzing dynamic properties and size distribution of small particles in solution. The major advantages are its rapid analysis and the simplicity of sample preparation.

After collision events between the monochromatic coherent beam of light and small particles, light scatters in all the directions (Rayleigh scattering). This process can occur if the dimension of the particles is smaller than the wavelength of the light. The scattering intensity fluctuates over time because the molecules in solutions undergo to Brownian motion, varying the distance between the particles involved in the scattering processes. This scattered light then undergoes either constructive or destructive interference by the surrounding particles, and within this intensity fluctuation, information is contained about the time scale of movement of the scatterers.

The dynamic information of the particles is derived from an autocorrelation function related to the fluctuating scattered intensity:

$$g_2(\tau) = \frac{G_2(\tau)}{\langle I \rangle^2}$$

Where ⟨I⟩ is the average intensity, τ is the correlation time and $G_2(\tau)$ is the temporal correlation function. $G_2(\tau)$ can be related, by means of the Siegert relation, to the electric field correlation function $g_1(q,\tau)$:

$$g_1(\tau) = \exp(-q^2 D\,\tau)$$

where q is the magnitude of the scattering vector and D is the translational diffusion coefficient. By using the Stokes-Einstein equation it is possible to obtain the hydrodynamic radius as:

$$D = \frac{\mathrm{kT}}{6\pi\eta R_h}$$

where D is the diffusion coefficient (m^2s^{-1}), k is the Boltzmann's constant (JK^{-1}), T is the temperature (K) and η is the solvent viscosity (ms^{-1}).

The measurement was done with a Zetasizer nano series from Malvern®. The sample is measured using a clear, four-sided plastic cuvette. For sample analysis, the machine's software was used. Before the measurement a few parameters need to be set: the viscosity, the solvent type, and the particle material. It is important to notice that this type of analysis has been performed only for the bigger particles due to the low accuracy of that particular instrument. The measurements are considered accurate for particles with a diameter greater than 20 nm.

SEM

Scanning electron microscopy uses a focused beam of high-energy electrons to generate a variety of signal by scanning the surface of solid specimens. The signal derives from electron-sample interactions, revealing information about the sample, including external morphology (texture), chemical composition, and crystalline structure and orientation of materials making up the sample. The signals produced when accelerated highly energetic electrons hit the solid sample includes: secondary electrons, backscattered electrons (BSE), X-ray photons, visible light and heat.

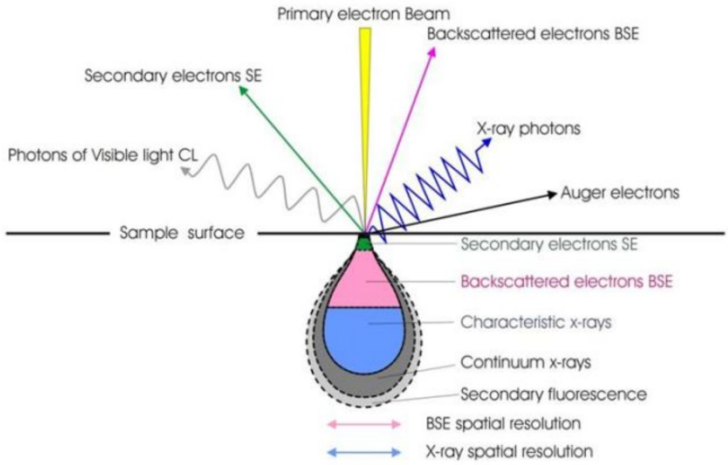

Figure 4. In a SEM, electrons interact with a sample's atoms

Secondary electrons and backscattered electrons are commonly used for imaging samples: secondary electrons are most valuable for showing morphology and topography on samples and backscattered electrons are most valuable for illustrating contrasts in composition in multiphase samples. X-ray photons are produced by inelastic collisions of the incident electrons with electrons

in discrete orbitals of atoms in the sample. As the excited electrons return to lower energy states, an X-ray is emitted with fixed wavelength, related to the difference in energy levels of electrons in different shells for a given element. Thus, characteristic X-rays are produced for each element as a consequence of the excitation due to the primary electron beam.
SEM analysis is considered to be non-destructive: x-rays generated by electron interactions do not lead to volume loss of the sample, so it is possible to analyze the same materials repeatedly.
The measurements presented in this work are made with FEI Nova NanoSEM 230, and this type of analysis is performed only for BGNP, because the SGNP are too small to be distinguished by the instrument.

AFM

The atomic force microscope system is a useful tool for direct measurements of intermolecular forces with atomic-resolution characterization that can be applied in a broad spectrum of application[19].
The AFM system consists of a micro-machined cantilever probe and a sharp tip, connected to a sensitive photo detector that act as a feedback system to deflect the cantilever according to a signal produced when laser beam is reflected off.
The tip is scanned over the sample surface, and the shift from its natural resonance frequency due to sample attractive interaction is measured to obtain topographical information. In fact, the photon beam hits the back part of the cantilever in correspondence of the tip and it reflects on a photodetector, able to detect different reflection angles, from which the exact height of the tip (and consequently of the sample) can be evaluated. The final result is a color map of the sample surface that indicates the height of each point of the surface. It is easy to understand the importance of having a super flat surface on which the sample is placed. This role is played by the mica, that can accomplish the need of a surface with a very low roughness.
In this work, GNPs are observed and measured using a Bruker MultiMode AFM. This technique, in this thesis, is utilized only for SGNP, because SEM technique, used to size BGNP, is not applicable for SGNP.

TEM

Transmission electron microscopy is a microscopy technique in which a beam of electron is transmitted through a specimen to form an image.

A high energy beam of electrons is transmitted through a very thin sample, and the interactions between the electrons and the atoms can be used to characterize the specimen, obtaining information about crystal structure and defects in the structure, such as dislocations and grain boundaries. Chemical analysis can also be performed. TEM can be used to study the growth of layers, their composition, and defects in semiconductors.

During the transmission, the speed of electrons can be directly correlated to the electron wavelength: the faster electrons move, the shorter the wavelength, and the greater the quality and detail of the image. The lighter areas of the image represent the places where a greater number of electrons were able to pass through the sample, and the darker areas correspond to the dense areas of the object. These differences provide information on the structure, texture, shape and size of the sample.

Since the electron beam has to pass through, the specimen was put on an ultra-thin carbon grid in a very low concentration. For this reason, the samples are diluted 100 times and just few microliters are placed on the grid. The results presented here are obtained also with TEM for both SGNPs and BGNPs. The measurements were performed at Rice University (Houston, TX) in the department of mechanical engineering with a JEOL 1230 High Contrast Transmission Electron Microscope.

Z Potential

Zeta potential is a tool for understanding the state of the nanoparticle surface and predicting the long-term stability of the nanoparticle. In fact, it is a technique used to determine the surface charge of nanoparticles in solution.

From a theoretical point of view, the Z potential is the electrical potential difference between an interfacial electrical double layer (EDL), it means that in the presented system, the Z potential

corresponds to potential difference between the dispersion medium and the stationary layer of fluid attached to the dispersed particle.

The surface of the particles is negatively charged, and positive charges already present in the solution will accumulate in its vicinity forming a charged shell around the particle. In the charged shell, there will be an inner layer in close proximity with the solid surface where the ions will be stronger bounded (first layer) and an outer layer in which the ions undergo to a reduced influence of the particle. Here, the electrostatic potential exponentially decreases while increasing distance from the surface of nanoparticles, into the bulk solution, in which the potential is considered as the reference one. As a consequence, the charges in the second layer are subject to diffusion. This phenomenon is shown in Fig. 4.

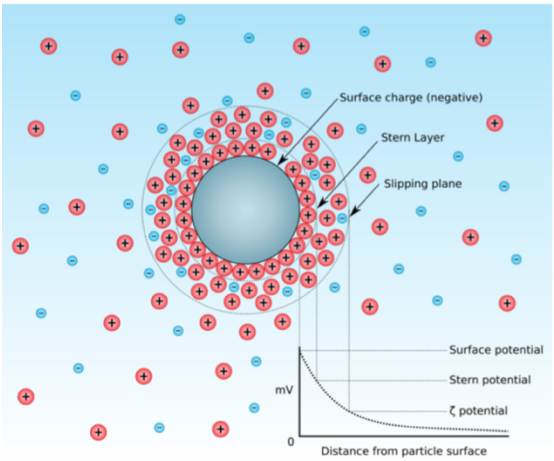

Figure 4. Graphical representation of the EDL around a negatively charged particle and zeta potential

The arrangement of charges at the interface is the electrical double layer (EDL). According to external stimuli, as an electrical field or a pressure difference, a set of electrokinetic effects occur due to the relative movements of the ionic layers: electrophoresis, electro-osmosis, streaming potential and sedimentation potential. The electrophoresis occurs when an electric field is applied between two different electrode, the system is shown in fig. 5, causing to the charged particles to move towards the opposite electrode. Within this diffuse layer there is a hypothetical plane which acts as the interface between the moving particles and the layer of dispersant around it while

electrophoresis. This plane is the characteristic slipping/shear plane and Z potential is the potential at this particle-fluid interface[20].

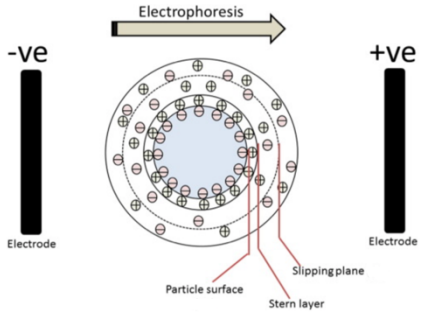

Figure 5. External electric field applied to measure Z potential at a particle surface

Z potential cannot be measured directly and is deduced from electrophoretic mobility (μ_e) of charged particles under an applied electric field.

$$\mu_e = \frac{V}{E}$$

where V is particle velocity (μm/s), E is electric field strength (Volt/cm). The Z potential is then calculated from the obtained μ_e by the Henry's equation:

$$\mu_e = \frac{\varepsilon_r \varepsilon_0 \zeta f(KA)}{3\eta}$$

where ε_r is relative permittivity/dielectric constant, ε_0 is permittivity of vacuum, ζ is Z potential, f(Ka) is Henry's function and η is viscosity at experimental temperature. Henry function can be approximated by two possible values: 1.5 which is the Smoluchowski approximation, used for particles greater than 0.2 μm or 1.0 which is the Huckel approximation, applied for smaller particles.

The zeta potential determines many of the colloidal properties such as adsorption capabilities or interaction energy between particles. This can be correlated to the stability of the particles against coagulation or with the sedimentation behavior of the colloidal itself.

The most important quantity that affects the zeta potential is the pH. In fact, considering negatively charged particles in suspension (negative zeta potential), if more alkali is added, the solution will become more basic and the particles will acquire a more negative charge, increasing, in absolute value, the zeta potential. On the contrary, if acids are added, more positive charges will be present neutralizing the particles charge. This condition is the so called isoelectric point. Generally speaking, if a colloidal system has a zeta potential $|\zeta| \geq 30$ mV is considered stable.
The measurements here presented are done for both SGNP and BGNP. The sample is inserted in a clear, four-sided plastic cuvette equipped with a special cap with electrodes. After the electric potential is applied, electrophoresis mobility is measured through the Laser Doppler Velocimetry (LDV). In this technique, a laser beam hits the cuvette and the scattered light is detected at an angle of 17°. The scattering is combined with the reference beam, producing a fluctuation in the intensity of the scattered light, whose rate is proportional to the speed of the particles.
The instrument used for this characterization is a Zetasizer nano series from Malvern®, each measure has 5 replicates in 10 mM KCl solution and the result is reported as mean ± SD.

UV-vis spectrometer

Ultraviolet-visible spectrometry measures the intensity of light passing through a sample and compares it to the intensity of light before it passes through the same sample.
A beam of light from a visible and/or UV light source is separated into its component wavelengths by a prism or diffraction grating. Each monochromatic (single wavelength) beam in turn is split into two equal intensity beams by a half-mirrored device. One beam, the sample beam, passes through a small transparent container containing a solution of the compound being studied in a transparent solvent. The other beam, the reference, passes through an identical cuvette containing only the solvent. The intensities of these light beams are then measured by electronic detectors and compared. The intensity of the reference beam, which should have suffered little or no light absorption, is defined as I_0. The intensity of the sample beam is defined as I. Over a short period of time, the spectrometer automatically scans all the component wavelengths in the manner described. The ultraviolet (UV) region scanned is normally from 200 to 400 nm, and the visible portion is from 400 to 800 nm. If the sample compound does not absorb light of a given wavelength, $I = I_0$. However, if the sample compound absorbs light then $I<I_0$.
As a result of the detectors, the instrument will measure the ratio between I and I_0 passing through the cuvette, evaluating in this way the transmittance, from which the absorbance can be derived:

$$A = -\log\left(\frac{I}{I_0}\right)$$

Since from the literature the maximum absorbance of Au colloidal is around 550 nm, the wavelength range was set between 200 nm and 800 nm.
Optical analysis was performed with an UV-Vis spectrophotometer located in the lab- oratory, by putting 500 µl of sample in a micro-cuvette with two clear sides.

ICP-MS and concentration analysis

Inductively coupled plasma mass spectroscopy is a type of mass spectroscopy which is capable of detecting metals and several non-metals at concentrations as low as one part in 1000. This is achieved by ionizing the sample with inductively coupled plasma and then using a mass spectrometer to separate and quantify those ions.
For coupling to mass spectrometry, the ions from the plasma are extracted through a series of cones into a mass spectrometer, usually a quadrupole. The ions are separated on the basis of their mass-to-charge ratio and a detector receives an ion signal proportional to the concentration.
For the measurement, the sample has to be completely dissolved. For this reason aqua regia (3:1HCl:HNO3) is synthesized and used to dissolve GNPs. This is further diluted in 2% HCl. Then, a calibration curve is built considering 5 points around the hypothetical concentration of the sample. A gold standard, with a known nominal concentration of 1000 µg/ml, is used to create different dilutions to make the standard curve to calibrate the instrument. The final concentrations of the standard sample are: 10 µg/l, 50 µg/l, 500 µg/l, 5000 µg/l and 10000 µg/l. After the a calibration curve is obtained, measurements from different unknown samples can be calculated using the standard curve fit to determine their concentration.
This type of analysis is performed using a Perkin Elmer Nexion 300 ICP-MS at Rice University (Houston, TX) in the Bioscience Research Collaborative building, where training for use of the instrument and sample preparation was done.
Both SGNPs and BGNPs are tested with this technique to analyze the concentration of the synthetized nanoparticles. Measurements are made to support the theoretical prediction of concentration, based on the work of Haiss *et al*[21]. They propose an equation suitable for the

determination of the concentration of a colloidal solution starting from the size, the maximum absorbance of the sample and a few other parameters:

$$d = \left(\frac{A_{spr}(5.89 \times 10^{-6})}{c_{Au} \exp(C_1)}\right)^{1/C_2}$$

Where A_{spr} is the plasmon resonance absorbance, d is the diameter of the particles (nm) and c_{Au} is the concentration of the sample (mol/L). C_1 and C_2 are constants evaluated experimentally. Plotting the linear behavior of the extinction coefficient at the surface plasmon resonance by varying the particle diameter, C_1 and C_2 are defined as the intercept and the slope of the line, respectively. The values of the constants are set equal to the theoretical one: C1 = −4.70 and C_2 = 0.3. In this work the diameter of the nanoparticle, obtained from the previous presented techniques, is exploited to evaluate the concentration of the samples.

3.2 Lewis Lung Cells

The Lewis carcinoma is a mouse lung tumor studied by Dr. Margaret R. Lewis in 1951. Some of the primary cells had been isolated and a new cell line started (LLC1). Being highly tumorigenic for C57/BL6 mice, they are often used to induce tumors for antitumoral treatments studies.
Murine Lewis lung cells (LLC1) are purchased from ATCC® (Manassas, VA, USA) and subcultured according to manufacturer's recommended protocols. Cells are made to express luciferase (becoming LLC-luc) by the use of plasmid pLenti PGK V5-LUC Neo[22] (Addgene, Cambridge, MA, USA) which is packaged in lentiviral particles. To visualize luminescence, D-Luciferin, Sodium Salt (Gold Biotechnology, St. Louis, MO, USA) is prepared and used according to the following reported protocols. Cells were kept at 37 ^{0}C and 5% humidity in HERAcell 150i CO2 incubator (ThermoFisher Scientific, Waltham, MA, USA).

3.2.1 Cell Culture

For the culture of this cell line Dulbecco's Modified Eagle's Medium (DMEM, ATCC®, Manassas, VA, USA) is made complete by adding 10% fetal bovine serum (FBS, USDA approved, ATCC®,

Manassas, VA, USA) and 1% Geneticin™ (ThermoFisher Scientific, Waltham, MA, USA) to maintain the expression of luciferase for each subculture. LLC-luc cells are cultured in flasks with 75 mm^2 surface area (T75) and periodically split when the coverage percentage of the flask surface is around 85%-90%. LLC-luc cells appear rounded, slightly attached to the surface and have a population doubling time of about 21 hours. They tend to grow as a single layer on the plastic surface and if the coverage reaches 100% they start to generate multilayers creating a non-healthy environment and cells to death. Each subculture is considered as a new subsequent generation (passage) of cells.

The subculture is performed under a sterile hood to avoid contamination and both the hood the gloves of the operator have to be sprayed with ethanol for bacteria disinfection. The process is constituted by the following steps:

- With the help of an aspirator connected to the vacuum line in the hood, all the media is removed from in the flask
- The flask is washed with 10 mL of 1X Phosphate Buffered Saline (PBS) to ensure complete removal of media, PBS is then removed with the vacuum line after gently shaking the flask
- 2 ml of 1X Trypsin-EDTA (Ethylenediaminetetraacetic acid) 0.25% are added to the flask and placed in the incubator for 5 min. The trypsin dissociates the cell-cell and cell-flask interactions, completely detaching the cells. Note that the trypsin is quite toxic for the cells. To help the process, the flask can be gently shaken.
- With a serological pipet the cells are collected from the flask and combined in a 50 ml centrifuge tube, adding DMEM media in a volume at least equal to that of the trypsin
- After mixing, 10 µl of cells are placed in a 0.5 ml eppendorf tube with 10 µl of trypan blue, a dye used to stain the cells
- After mixing, 20 µl of the cell solution is removed and pipetted onto a slide for cell counting
- Counting is performed with a Cellometer® from Nexcelom Bioscience. This instrument gives the number of living cells per milliliter. The number of cells in the entire volume is evaluated and the appropriate amount of cells is removed to create a new cell passage. For a T-75 flask the amount used

was 8.25×10^5 cells per flask

- Remaining cells are centrifuged at 200 G for 10 min
- Supernatant is discarded and the cells are mixed with a freezing media composed by 95% Fetal Bovine Serum (FBS) and 5% Dimethyl sulfoxide (DMSO). The DMSO will cryopreserve and stabilize the cells especially in the future thawing phase
- Cells are stored in cryotubes at -80 °C. In order to avoid thermal shock, cryotubes are initially inserted in a plastic box containing isopropanol alcohol (IPA) that allows for a decreasing temperature at a rate of 1 °C/min.

3.2.2 LLC Luciferase gene expression

Lewis Lung cells are engineered to express the firefly luciferase gene for subsequent *in vivo* bioluminescence imaging. The expression is an important tool not only for the detection of the labeled cells and cancer progression *in vivo*, but also for the verification of proliferation of a certain cell line *in vitro*.

Cells were made to express luciferase by the use of plasmid pLenti PGK V5-LUC Neo26 (Addgene, Cambridge, MA, USA) which is packaged in lentiviral particles. The packaging is performed at the Baylor College of Medicine (BCM) vector core facility. The plasmid is transfected into Human Embryonic Kidney (HEK-293T) cells, and the conditioned media collected and used to infect the LLC1 for 24h. After 24h, selection is initiated with G418 (Geneticin, ThermoFisher Scientific, Waltham, MA, USA).

To stabilize the new cell line, several passages are subcultured prior to *in vitro*, *in ovo* and *in vivo* experimentation. Furthermore, they are cultured in the usual media with the addition of 1% Geneticin, an antibiotic selective for the non-luciferase expressing cells. In this way, the expression is guaranteed also in future cell generations

3.2.3 *In vitro* test and related equipment

Proliferation Test

Cell proliferation is an increase in the number of cells resulting from the normal, healthy process by which cells grow and divide. In this regard, cell proliferation can be a good indicator of general cell health. Cells that are subject to a variety of disease states may exhibit different rates of proliferation than normal cells.

In this study, cell proliferation tests are performed to ensure maintained expression of the luciferase gene by the cells after several subculture passages. To visualize luminescence, D-Luciferin, Sodium Salt (Gold Biotechnology, St. Louis, MO, USA) is first dissolved in Phosphate Buffered Saline without calcium and magnesium (PBS, ThermoFisher Scientific, Waltham, MA, USA) and filtered using a 2 µm filter under sterile conditions prior to use. Then, 1 µl of 30 mg/ml luciferin is added to each well of a 96-well plate containing 200 µl of cells and media. The plate is placed in a Xenogen Caliper Spectrum In Vivo Imaging System (IVIS, Perkin Elmer, Waltham, MA, USA) to verify bioluminescence, and the luciferase gene expression prior *in vitro*, *in ovo* and *in vivo* testing. D-Luciferin solution is added immediately prior to the imaging process to ensure the activation of the bioluminescence reaction[23]. the luminescent cells are excited with a light source, and the emitted light is collected by a CCD camera that allows the reconstruction of the image. The instrument used for this purposed is the IVIS, shown in fig. 6.

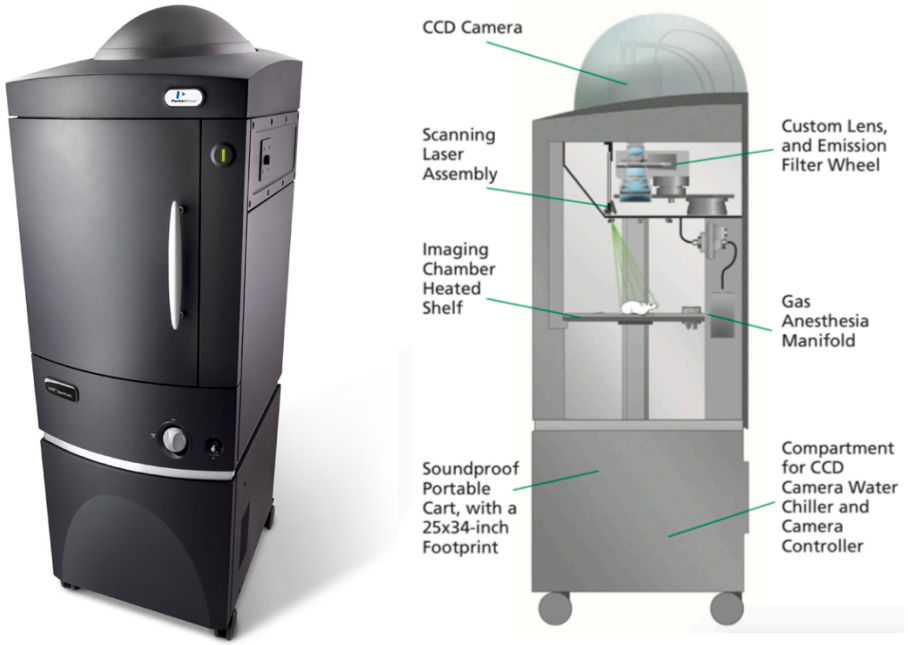

Figure 6. Picture of IVIS and schematic of its more important components

The software superimposes the optical image (in gray scale) taken by a normal camera and the luminescence signal, represented by a color scale. The unit of measurement is photon/sec/cm^2/sr, with which is possible to compare images with different exposure time. For all the experiments here reported the exposure time is settled on automatic (the instrument chooses the right exposure time according to the bioluminescent signal of the sample, avoid over or under exposure. The amount of signal is proportional to the number of live luciferase expressing cells, where the greater the number of cells, the higher is the signal detected by the system.
In the post-processing, the image is analyzed, and to evaluate the data and the corresponding outcome, a circle with fixed diameter is drawn onto the image and the bioluminescence signal contained in the area inside the circle is measured. This area is referred to as the Region of Interest (ROI).

Comet Assay

The single cell gel electrophoresis assay (SCGE, also known as comet assay) is an uncomplicated and sensitive technique for the detection of DNA damage at the level of the individual eukaryotic cell. It was first developed by Östling & Johansson in 1984 and later modified by Singh *et al*. in 1988. The comet assay (single-cell gel electrophoresis) is a simple method for measuring deoxyribonucleic acid (DNA) strand breaks in eukaryotic cells. Cells embedded in agarose on a microscope slide are lysed with detergent and high salt to form nucleoids containing supercoiled loops of DNA linked to the nuclear matrix. Electrophoresis at high pH results in structures resembling comets, observed by fluorescence microscopy. The term "comet" refers to the pattern of DNA migration through the electrophoresis gel, which often resembles a comet. The intensity of the comet tail relative to the head reflects the number of DNA breaks. The likely basis for this is that loops containing a break lose their supercoiling and become free to extend toward the anode. This is followed by visual analysis with staining of DNA and calculating fluorescence to determine the extent of DNA damage. This can be performed by manual scoring or automatically by imaging software.
A Neutral Comet Assay is performed on LLC-luc cells using a CometAssay® Kit (Trevigen, Gaithersburg, MD, USA) as per manufacturer's instruction to detect DNA damage due to irradiation.
Briefly LLC-luc are incubated with 54.5 µg of either SGNP or BGNP for 48 hr and irradiated with 2 Gy using a Rad Source RS-2000 Biological Research Irradiator (Buford, GA, USA). Thirty

minutes after irradiation cells are collected, counted, and mixed with 0.5% low melting point (LMP) agarose and spread over the comet slide. Afterwards, the slides are immersed for at least 1 h in ice-cold freshly prepared lysis solution. The slides are than removed from lysis solution and placed in a cold 1x neutral electrophoresis buffer for 30 minutes. Horizontal electrophoresis is performed at 4°C under dim light for 45 min at 21 V. After electrophoresis, the slides are immersed in DNA Precipitation Solution for 30 minutes and 70% ethanol for 30 min at room temperature. Each slide is air dried and stained with 1x SYBR® Gold Staining Solution (Trevigen, Gaithersburg, MD, USA) in the dark. All slides are washed with water and air dried. Samples are visualized using an EVOS FL Auto microscope (Life Technology). To quantify the DNA damage, tail length (TL) and tail moment (TM) are evaluated. Tail length (length of DNA migration) is related directly to the DNA fragment size and presented in micrometers. It is calculated from the center of the cell. Tail moment is calculated as the product of the tail length and the fraction of DNA in the comet tail. At least 50 random cells are scored per sample. Image is analyzed by Open Comet plugin in ImageJ for various comet parameters[24].

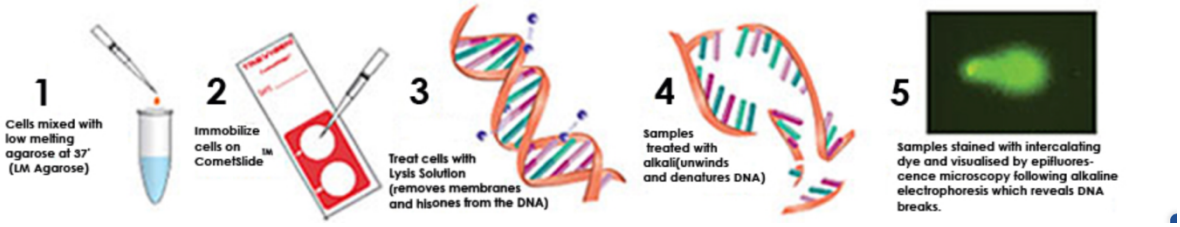

Figure 7. Experimental procedure of Comet Assay

Clonogenic Assay

In 1956, Puck and Marcus published a seminal paper describing a cell culture technique for assessment of the clone or colony forming ability of single mammalian cells plated in culture dishes with a suitable medium. The assays detect all cells that have retained the capacity for producing a large number of progeny after treatments that can cause cell reproductive death as a result of damage to chromosomes, apoptosis, etc[25].

Therefore, the Clonogenic assay is the method of choice to determine cell reproductive death after treatment with ionizing radiation but can also be used to determine the effectiveness of other cytotoxic agents. Only a fraction of seeded cells retains the capacity to produce colonies.

LLC1 cells are treated with 54.5 µg of either SGNP or BGNP for 48 hr followed by 2 Gy radiation of either cells alone or a combined treatment with NPs using a Rad Source RS-2000 Biological Research Irradiator (Buford, GA, USA). Thirty minutes after irradiation cells are trypsinized and approximately 200-500 cells from each sample were plated in triplicate in 6-well plates. After 10-15 days, the colonies are stained with 0.5% crystal violet solution in 50% methanol. Clonogenic efficiency is measured by % area and/or % intensity through colony area (ImageJ).

For both the Comet assay and Clonogenic assay a radiation equipment is used to irradiate the cells. The biological X-ray irradiator is, as reported above, the RS-2000 from RAD SOURCE with the concession of Mitra's research group from the Department of Radiation Oncology at the Houston Methodist Research Institute. The machine, shown in fig. 8, has a shielded X-ray tube without a radioactive source, so it can be considered safe for use. In the chamber some concentric circles are drawn, which correspond to different exposure fields. The sample to be irradiated is placed inside one of these circles according to the radiation dose that one wants to achieve.

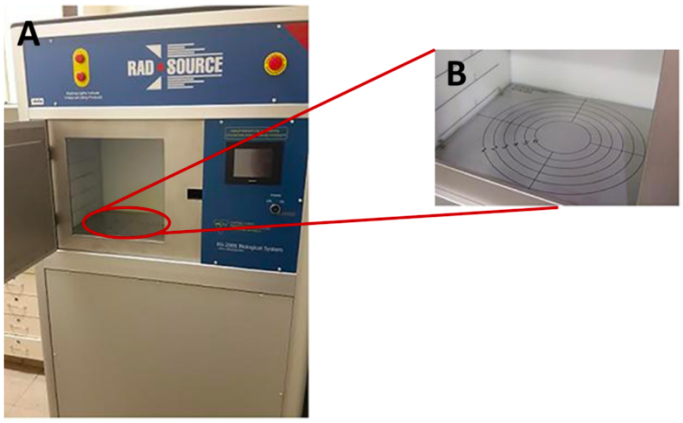

Figure 8. (A) Radiation equipment used for experiments, general view. (B): magnification of the internal part of the chamber. Note the circumferences that define the different zones for different doses

A summary table is represented in fig. 9. As an example, to irradiate an object with 2 Gy, the right the level has to be preselected (which in this case correspond to Level-0), and the object has to be located inside the corresponding circle (in this case the greatest). Finally, the time required to reach the desired dose (in the example about 30 s) has to be set.

Levels	Output (Gy/min)	Source distance (mm)	Field diameter (mm)
Level 7	59.0	118	75
Level 6	24.3	184	118
Level 5	13.5	247	63
Level 4	8.7	308	206
Level 3	5.9	373	250
Level 2	4.3	437	294
Level 1	3.3	501	337
Level 0	2.9	530	357

Figure 9. Table of the levels and corresponding outputs in Gy/min

The same machine was used for irradiation of both eggs and mice. Since the dose delivered to the eggs was always quite low, 6 eggs could be irradiated at a time thanks to the large irra- diation field. On the other hand, because of the high dose used for the mice (up to 20 Gy), it was possible to only irradiate two mice at a time due to the smaller circumference of the field. Furthermore, when mice were present, a lead partial body shield was used to protect the vital parts of the animals (head and body) and to irradiate only the flank.

3.3 Eggs

Eggs are purchased from Charles River (North Franklin, CT, USA) and maintained at 37°C with relative humidity set above 60%: they are 8 day old and specific pathogen-free embryonated. Eggs are prepared for inoculation with LLC-luc according to following procedure:

- open the shell with a needle between the two major vessels of the egg (they can be seen by illuminating the egg through the shell with an egg candler)
- air is pumped inside with a little rubber bulb in order to gently detach the membrane from the inner shell and to create an air sac underneath.
- a Dramel saw is used to create a window of 1 cm x 1 cm
- a silicone ring of 1 cm in diameter is place above the membrane. This will ensure a localization of the cells when inoculated
- a scotch tape is placed over the window to protect the egg[26]

Eggs are grafted with $1x10^6$ LLC cells in 40 µl PBS++ and 20 µl of basement membrane protein mixture (Matrigel, Corning, New York, USA) or LLC-luc cells with 7.56 µg of either 3.4 nm or 35 nm GNPs on day 8 after fertilization. The best time to incorporate the gold nanoparticles is at the same time as cells inoculation. In particular, the desired number of particles is suspended in a solution of cells, matrigel and PBS and then inoculated together, without changing the PBS/matrigel ratio.

The appropriate concentration of cells for 3D tumor growth was determined during prior experiments by first inoculating three eggs each with either $5x10^5$, $1x10^6$, or $2x10^6$ LLC cells to determine the optimal cell concentration for tumor growth.

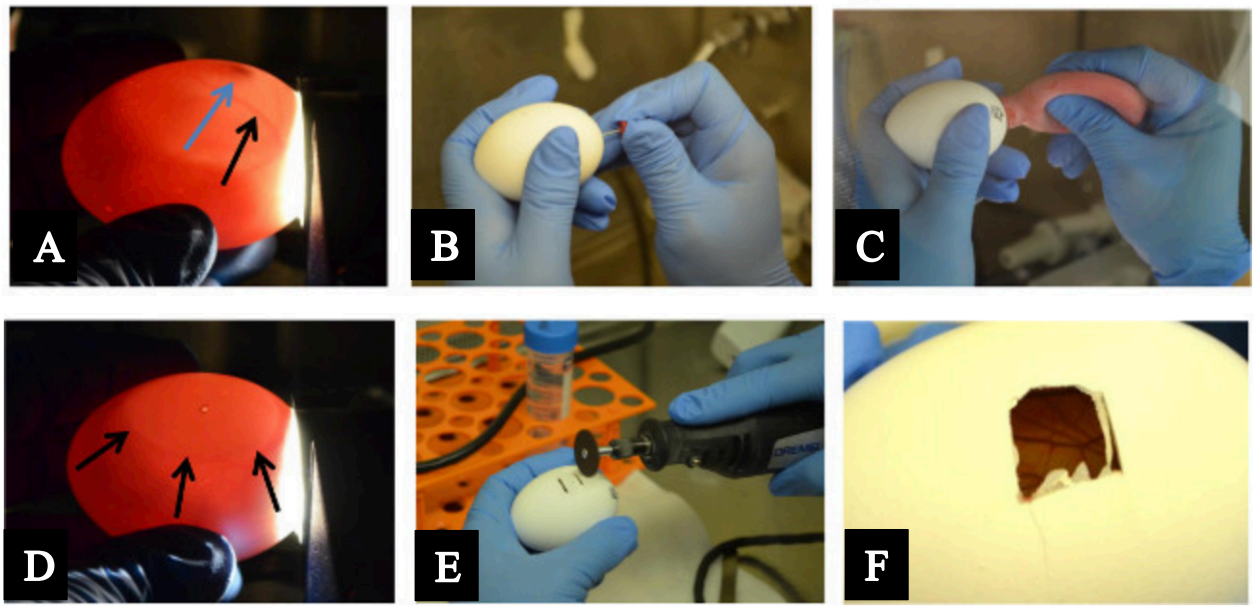

Figure 9. (A) Identification of embryo (blue arrow) and vessel (black arrow) using the candler. (B) The hole is made with the needle. (C) Creation of the air sac. (D) Verification of the successful dropping of the CAM away from the shell. Opening the window with the little saw and final result (E) and (F)

Eggs are irradiated with 2 Gy + 2 Gy on day 11 and 13 using a Rad Source RS-2000 Biological Research Irradiator (Buford, GA, USA). Eggs are than imaged with IVIS on days 11-14 after pipetting 100 µl of 15 mg/ml luciferin in PBS within the silicone ring five minutes prior to imaging. Experiments are ended on day 14 after fertilization. The tumor tissues are extracted from the CAM,

measured, weighed and processed for H&E. Tumors are fixed in 10% formalin and stored at 4°C prior to H&E or silver-enhanced staining.

3.4 Mice

All experiments are approved by the Institutional Animal Care and Use Committee (IACUC) at Houston Methodist Research Institute and are performed according to the principles of the NIH Guide for the Care and Use of Laboratory Animals, the provisions of the Animal Welfare Act, PHS Animal Welfare Policy, and the policies of the Houston Methodist Research Institute.
The mice are housed and cared for in accordance with the regulations of the Animal Welfare Act and recommendations of the Guide for the Care and Use of Laboratory Animals.
The mice are 6-week-old female C57/BL6 mice, which are purchased from Taconic Biosciences (Rensselaer, NY, USA).
When the weight of the mice is ~18.4 g (approximatively 7-week-old), the mice are inoculated in the right flank with $1x10^6$ cells in 100 µl of PBS, using a 28 gauge sterile insulin syringe, as shown in fig.10. During the injection the mice are sedated.

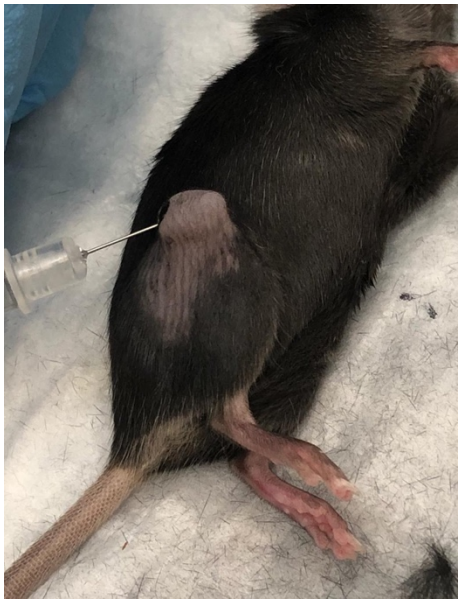

Figure 10. Inoculation of $1x10^6$ LLC-luc in the right flank of a mouse

Mice are weighed, and tumors measured daily using a caliper by measuring two dimensions in two different directions. Tumor volumes are calculated by squaring the minor axis dimension and multiplying it by the major axis and then diving the results by two.

To monitor the health of the mice also their body temperature is measured daily, using a rectal probe.

Mice are placed under anesthesia prior to irradiation. Mice are first placed in an isoflurane chamber with Fluriso (VetOne, Boise, ID, USA) to maintain a surgical plane. After about two minutes, artificial tears (LubriFresh P.M., Major® Pharmaceuticals, Livonia, MI, USA) are applied and animals are injected with 1 mg/kg Dexdomitor (Zoetis, Parsippany, NJ, USA) and placed back into the chamber for about two minutes or until their respiration slowed.

Prior to irradiation, mice are placed on a flat surface warmed using a heating pad, positioned and injected intratumorally along the longitudinal tumor axis with 9.37 mg of BGNPs (in a solution of ~100 µl) and shielded using a right flank shield (Precision X-ray Inc., North Branford, CT, USA). Mice are x-ray irradiated using a Rad Source RS-2000 Biological Research Irradiator (Buford, GA, USA) when their tumor size is ~281 mm^3. After irradiation the animals are given a reversal of 1 mg/kg Atipamezole (Zoetis, Parsippany, NJ, USA) and allowed to recover in an empty cage placed on a warm heating pad.

Prior to IVIS imaging (as shown in fig. 11), mice are also anesthetized using isoflurane and shaved on their right flank.

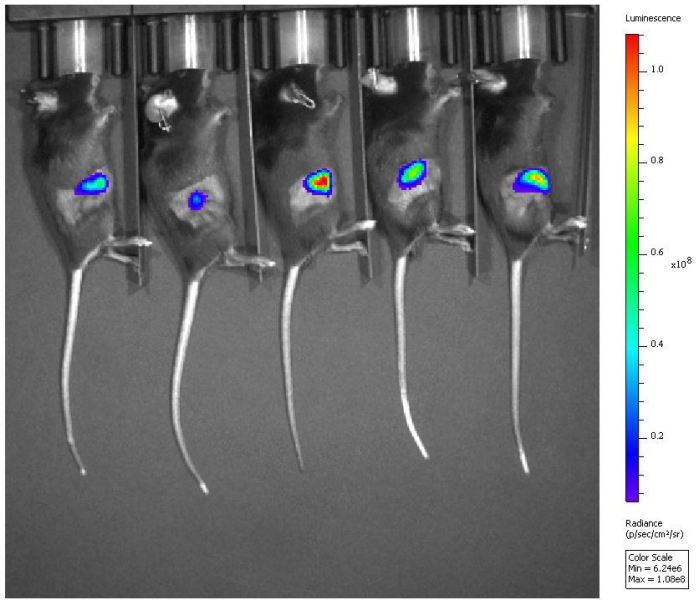

Figure 11. Mice in the IVIS during the imaging process

100 µl of 15 mg/ml luciferin in PBS is intraperitoneal injected ten minutes prior to imaging. Mice are IVIS imaged three times a week using autoexposure settings.
The mice are euthanized eight days after irradiation. The tumor and liver are harvested and processed for H&E. *Ex vivo* tumors are measured along three dimensions and their weight is also measured.

3.5 Histology

Histology, also known as microanatomy, is the study of the anatomy of cells and tissues of plants and animals using microscopy. The light microscope or electron microscope is used to study the specimen having been sectioned, stained, and mounted on a microscope slide.
Histological studies may be conducted using tissue culture, where live animal cells are isolated and maintained in an artificial environment for various research projects. In this case the artificial environment is composed by 10% formalin, and then alcohol. The ability to visualize or differentially identify microscopic structures is frequently enhanced through the use of staining. Histology is an essential tool of biology and medicine.
Hematoxylin and eosin stain or haematoxylin and eosin stain (H&E stain or HE stain) is one of the principal stains in histology. It is the most widely used stain in medical diagnosis and is often the gold standard.
Hematoxylin is a dark blue or violet stain that is basic/positive. It binds to basophilic substances (such as DNA and RNA, which are acidic and negatively charged). Instead Eosin is a red or pink stain that is acidic/negative. It binds to acidophilic substances such as positively charged amino acid side chains. This combination of staining processes leads to the observation, under the optical microscope, of the following color-element couple: nuclei are blue/purple, cytoplasm is red, DNA and RNA are violet, etc.
Silver-staining methods are helpful for histological identification of pathological deposits[27]. In this work it is used to visualize the GNP in the histologic samples of eggs and mouse tumor. The GNPs result as bright spots on a dark background.
The solutions which contains coloring agents used for silver-staining methods are usually colorless, and the simple application of these solutions to tissue sections, by itself, does not allow visualization through light microscopy even if the reagent has some affinity to the tissue elements.

Subsequent chemical transformation is necessary for visualization. Therefore, the attachment of silver ions to tissue elements is based on the *in situ* formation of silver salt, which, either in the solution or as salts, are reducible. They undergo reduction to form metallic silver. Some tissue elements exhibit an intrinsic reducing capacity, which may be strong enough to reduce silver ions into metallic silver particles *in situ*.
In this thesis the paraffin blocks are sliced and stained with Hematoxylineosin (H&E) and Silver Enhancer Kit, Silver Stain (Sigma Aldrich) by the pathology core of the Houston Methodist Research Institute. Slides are imaged for H&E with an Olympus IX81 inverted bright field microscope and with dark field microscopy using an oil objective on a Nuance Multispectral Imaging Microscope (Cambridge Research & Instrumentation).

3.6 Statistical analysis

GraphPad Prism 5 software is used for all statistical analyses.
Data are expressed as the mean ± s.e.m, which stands for standard error of the mean and it is the standard deviation of the population divided by the number of elements that composes the population. Asterisks included in the data graph are obtained statistically analyzing the data, and they represent the statistical significance. Statistical significance occurs when a result obtained from testing or experimentation does not occur randomly or by chance but is instead attributable to a specific cause. Statistical significance can be strong or weak, and it is important to discipline that rely heavily on analyzing data and research. To define how strong the significance is, P-values are used: the p-value or probability value or asymptotic significance is the probability for a given statistical model that, when the null hypothesis is true, the statistical summary (such as the sample mean difference between two compared groups) would be the same as or of greater magnitude than the actual observed results.
In this work to determine statistical significance the New England Journal of Medicine (NEJM) style is used; in this model there are three p-values and they are associated with different numbers of asterisks: *$p<0.033$, **$p<0.002$, and ***$p<0.001$.
Different types of analysis are performed on the data. The unpaired t-test with Welch's correction is performed on the Comet and Clonogenic assay data to compare between the treatment groups. The unpaired t test compares the means of two unmatched groups, assuming that the values follow a Gaussian distribution.

2-way ANOVA is used to analyze tumor growth in eggs and mice over time. 2-way analysis of variance (ANOVA) is an extension of the one-way ANOVA that examines the influence of two different categorical independent variables on one continuous dependent variable. The 2-way ANOVA not only aims at assessing the main effect of each independent variable but also if there is any interaction between them.

Chapter 4

Experimental design

4.1 Concentration of GNPs

4.1.1 UV-vis analysis

To calculate the concentration of the GNP solution, a UV-vis spectrometer is used. The following steps are performed in order to obtain the desired quantity:

- Different dilutions of the sample solution of GNPs are made, as shown in tab 1,2
- Each sample is analyzed by the UV-vis spectroscopy
- All of the absorbance curves are plotted together using MATLAB software
- The maximum absorbance value of each curve (value obtained in correspondence of ~534 nm of wavelength) is found for each dilution curve
- All the maximum points are interpolated with a function (usually power 2, with MATLAB)
- The equation of the fitting curve is used to find the value of the maximum absorbance for the undiluted solution
- This last value is used to determine the concentration of the undiluted solution, applying a formula based on the work of Haiss *et al.*21, reported in the Material and Methods section of this work (3.1.2 section)

This method is applied for both SGNPs and BGNPs. For BGNP samples, different dilutions are made when the sample is super concentrated (for example, when the absorbance peak saturates the

detector, or the solution is concentrated for injection into the mice tumor). The dilutions are reported in the following tables:

Dilution (number of fold)	GNP (μl)	MilliQ water (μl)
5	100	400
6	83.3	416.6
8	62.5	437.5
10	50	450
12	41.7	458.3
15	33.3	466.7
18	27.8	472.2
20	25	475

Table 1. Dilutions for both SGNP and BGNP solutions

Dilution (number of fold)	GNP (μl)	MilliQ water (μl)
18	27.8	472.2
20	25	475
22	22.7	477.3
28	17.9	482.1
30	16.7	483.3
34	14.7	485.3

Table 2. Dilutions for concentrated solutions of BGNP

4.1.2 ICP-MS

To support the concentration values obtained from the UV-vis data, IC-MS analysis is performed on different samples of both SGNP and BGNP solutions.

Table 3 lists the of samples on which the ICP-MS analysis was performed.

Sample #	Date on which GNP are made	Type of GNP	Diameter (nm)	Theoretical concentration (g/l)
1	11/03/17	SGNP	5.62	0.1236
2	02/19/18	BGNP	36.8	0.0794
3	02/19/18	BGNP	36.8	3446.4
4	11/03/17	SGNP	5.62	0.1212
5	01/15/18	BGNP	34.36	0.4402
6	01/15/18	BGNP	34.36	2298

Table 3. List of ICP-MS samples

Samples #3 and #6 are concentrated samples, obtained after the centrifugation and the removal of the supernatant of the starting solution.
Samples #1 and #4 are the same samples, measured at different times.

4.2 *In vitro* experiments

4.2.1 Proliferation tests on LLC-luciferase expressing cells

LLC cells are engineered to express luciferase, and at each passage, it is necessary to ensure the expression of luciferase and the healthiness of cells before inoculating them in eggs and mice.
In other words, there is the need to ensure that the luciferase expression persists also in the progeny of the engineered ones, evaluating the growth curve of the LLC-luc cells. This is done by exploiting the bioluminescence of the cells using IVIS imaging.
The LLC-luc cells are cultured in a 96-wells plate with different starting numbers of cells:

- Group 1: 6.25×10^3 cells
- Group 2: 3.125×10^3 cells

Each group is tested in triplicate.
IVIS images are acquired during the next 6 days in order to monitor the signal. In this case the ROI is used to evaluate the bioluminescent signal coming from a fixed area (circle).

4.2.2 Cellular uptake *in vitro*

This study is performed to verify the internalization of SGNP and BGNP by the cells. The sample preparation is performed through the following steps:

- Seed of $3x10^5$ LLC-luc cells in triplicate wells of a 6-well plate with 4 ml of media (DMEM)
- Wait 24 h
- Add (A) 26.9 μg or (B) 40.8 μg or (C) 54.5 μg of gold in each well
- Wait 24 h, without change the media
- Wash each well twice with PBS
- Detach the cells with trypsin (0.5 ml of trypsin for each well)
- Add media (1 ml for each well)
- Centrifuge (100G x 10 min)
- Remove the supernatant
- Add 1 ml of fixing agent for each sample (each well is a different sample)

Both SGNPs and BGNPs are tested in this study, and for each of them three different amounts of gold are tested, as reported above (A, B and C in the third step). To visualize the internalization TEM images are performed on the samples

4.2.3 Comet assay

LLC-luc cells are tested to evaluate the amount of DNA damage caused by the GNP, by the radiation alone and by the combined use of radiation and GNP. The test is performed for both SGNP and BGNP.
Passage 17 of LLC-luc is tested. Cells are cultured in T25 flasks (surface area of 25 mm^2) and treated with 54.5 μg of gold, which corresponds to:

- 157.9 μl of SGNP (with a concentration of 0.345 g/l)
- 198.2 μl of BGNP (with a concentration of 0.275 g/l)

Cells and GNP are incubated for 24 hours. After that different groups are created and tested.
Treatments groups include:

- Untreated (UT): cells alone
- Small gold nanoparticles (SGNP): cells treated with SGNP
- Big gold nanoparticles (BGNP): cells treated with BGNP
- Radiation alone (XRT-2Gy): cells treated with 2Gy
- Radiation + SGNP (SGNP XRT-2Gy): cells treated with SGNP and 2Gy
- Radiation + BGNP (BGNP XRT-2Gy): cells treated with BGNP and 2Gy

4.2.4 Clonogenic assay

LLC-luc cells are tested to evaluate the interruption of clonogenic activity of cell colonies due to radiation therapy, monitoring the reproduction rate of the cells in a Petri dish. The percentage of the plate area covered by the cells will be evaluated. The test is performed for both SGNP and BGNP.

Passage 17 of LLC-luc is tested. Cells are cultured in T25 flasks (surface of 25 mm^2) and treated with 54.5 μg of gold, which corresponds to:

- 157.9 μl of SGNP (with a concentration of 0.345 g/l)
- 198.2 μl of BGNP (with a concentration of 0.275 g/l)

Cells and GNP are incubated for 24 hours. After that different groups are created and tested. Treatments groups include:

- Untreated (UT): cells alone
- Small gold nanoparticles (SGNP): cells treated with SGNP
- Big gold nanoparticles (BGNP): cells treated with BGNP
- Radiation alone (XRT-2Gy): cells treated with 2Gy
- Radiation + SGNP (SGNP XRT-2Gy): cells treated with SGNP and 2Gy
- Radiation + BGNP (BGNP XRT-2Gy): cells treated with BGNP and 2Gy

4.3 *In ovo* experiments

Since, to the best of our knowledge, this is the first time that murine LLC-luc cells are inoculated on the CAM, preliminary experiments are performed in order to generate an effective protocol for this cell line. In fact, the final degree of vascularization, shape, and dimension of the tumor can be cell line dependent26. The number of initial cells inoculated on CAM is not directly proportional to the final dimension of the tumor. According to their distribution, the cells can form a nice nodule (especially if they are near vessels) or can form just a small nodule that falls into a sheet. There is no way to predict the final tumor shape. On the other hand, as a result of previous experiments and the wide experience of Dr. Pathak, it can be said that, once the optimal cell number is found, the same type of growth is expected for future experiments. Three different number of cells are tested: 0.5x106 cells, 1x106 cells, and 2x106 cells. From this preliminary test with 1x106 cells, it is possible to obtain a nice 3D tumors three day after inoculation. Preliminary tests are also made to optimize the amount of gold inoculated in the eggs. The treatment groups are the following:

- Untreated (UT): eggs bearing the tumor are not treaded
- Radiation alone (XRT-2GY+2GY): eggs are treated with two radiation doses of 2Gy (radiation occurs on day 0 and day 2)
- Small gold nanoparticles (SGNP-2GY+2GY): eggs are treated with SGNP and two radiation doses of 2 Gy (radiation occurs on day 0 and day 2)
- Big gold nanoparticles (BGNP-2GY+2GY): eggs are treated with BGNP and two radiation doses of 2 Gy (radiation occurs on day 0 and day 2)

The amount of gold in each egg is 7.56 μg for both SNGPs and BGNPs. Eggs are also tested, with the same groups reported above with 15.13 μg, but the results will not be reported because this amount of gold is revealed to be disruptive to tumor growth in the eggs.

4.4 *In vivo* experiments

All of the *in vivo* experiments are performed in the full compliance of the ethical principles and upon approval of the protocols by the Institutional Animal Care and Use Committee (IACUC).
In all of the following experiments, female black C57/BL6 are used and tumors growth is induced by injecting subcutaneously in the right flank of the mouse 1x106 LLC-luc cells suspended in 100 μl of PBS.
All of the experiments performed on mice involves only the use of BGNPs.

4.4.1 Preliminary experiment

A preliminary experiment is made to optimize the radiation dose: the amount of radiation needed to be effective, but not effective enough to completely suppress the radiosensitization effect of gold. Also, the mouse health is evaluated thought this preliminary experiment. In the preliminary experiment 40 mice are tested.

When the average weight of the mice is ~ 18.4 g (which correspond to 6-week-old mice), each mouse is injected with $1x10^6$ LLC-luc cells. Mice are weighted, and the tumor is measured every day. When tumors volumes are ~ 200 mm^3, mice are sorted in groups.
The treatments groups include:

- Untreated (UT): mice are not subjected to irradiation
- 12 Gy: mice are irradiated with a dose of 12Gy
- 16 Gy: mice are irradiated with a dose of 16Gy
- 20 Gy: mice are irradiated with a dose of 20Gy

The same experiment is performed involving both irradiation and the BGNPs. In each mouse 100 µl of BGNP is injected intratumorally right before the irradiation and the concentration of the GNP solution is 2.59 g/l.
The treatments groups are:

- 12 Gy+BGNP: mice are irradiated with a dose of 12Gy and BGNP
- 16 Gy+BGNP: mice are irradiated with a dose of 16Gy and BGNP
- 20 Gy+BGNP: mice are irradiated with a dose of 20Gy and BGNP

All of the mice are imaged every other day with IVIS in order to monitor the tumor growth behavior. Tumors are also manually measured every day. Eight days after treatment mice are euthanized and the tumor and liver of each mouse are collected. Ex vivo tumors are weighted before processing them for histology or ICP-MS. Half of the tumors and livers are immersed in 10% formalin to be conserved for histologic analysis. The other half of the tumors and livers are immediately immersed in liquid nitrogen to be flash frozen for ICP-MS analysis. Each half is randomly chosen.
Another preliminary experiment is performed to monitor the body temperature of mice for different treatment groups over time.
1x106 LLC-luc cells are injected in the mice when their weight is ~18.3 g and when the tumor volumes are ~ 181 mm3, mice are divided into different treatment groups, as following:

- Untreated (UT): mice are not subjected to irradiation

- 12 Gy only: mice are treated with 12 Gy of irradiation
- 12Gy+BGNP: mice are treated with 12 Gy of irradiation and BGNP

The mice treated with BGNPs receive a pre-irradiation injection of 100 μl of BGNP solution, where the amount of gold is equal to 215 mg (the concentration of the solution is 2150 g/l).
Body temperature is measured every day for each of the 37 mice involved in the experiment. As performed in the other preliminary experiments, after 8 days of treatments ex vivo tumors and livers are collected and processed to be conserved for histology and ICP-MS analysis.

4.4.1 Mice experiment

To evaluate the effectiveness of the radiosensitization of BGNP *in vivo,* 45 mice are tested.
As the preliminary experiment, when mice are injected with $1x10^6$ LLC-Luc their average weight is ~ 18.3 g (which correspond to 6-week-old mice). Mice are weighted, and the tumor is measured every day. When tumors volumes are ~ 181 mm^3, mice are sorted in groups, as report here:

- Untreated (UT): mice are not subjected to irradiation
- 12 Gy only: mice are treated with 12 Gy of irradiation
- 12 Gy + BGNP: mice are treated with 12 Gy of irradiation and BGNP

The mice treated with BGNP receive an injection pre-irradiation of 100 μl of BGNP solution, for an amount of gold equal to 215 mg (the concentration of the solution is 2150 g/l).
Body temperature is measured every day for each of the 37 mice involved in the experiment. As performed in the other preliminary experiments, after 8 days of treatments ex vivo tumors and livers are collected and processed to be conserved for histology and ICP-MS analysis.

Chapter 5

Results and discussion

5.1 GNP characterization

Two different sized gold nanoparticles small (SGNP) and big (BGNP) are synthesized and investigated for radiosensitization effects.

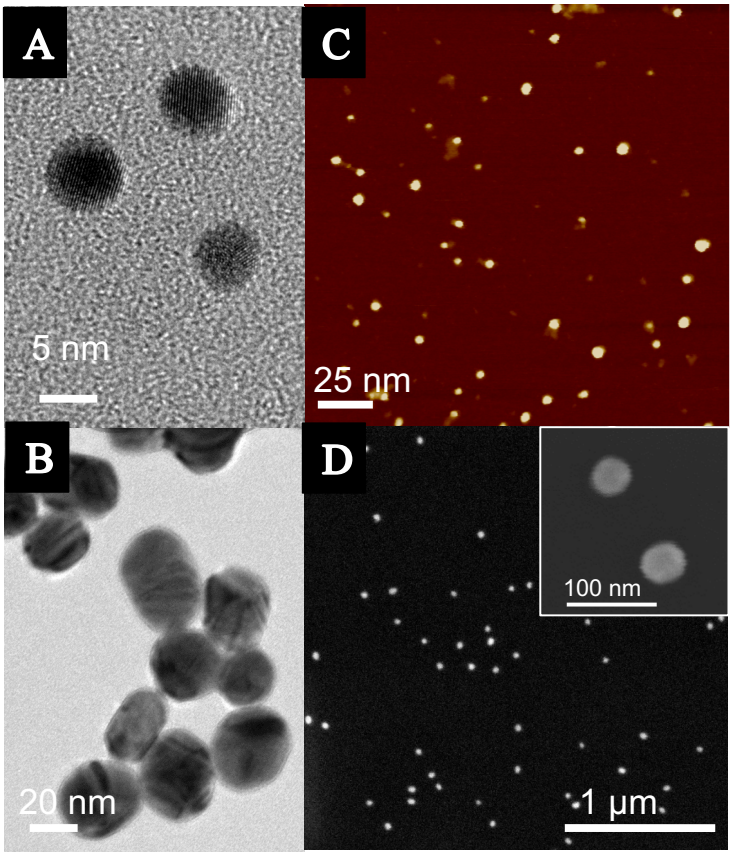

Figure 12. TEM images of (A) SGNP and (B) BGNP. (C) AFM image of the SGNP and (D) SEM image of the BGNP

SGNP are observed and measured on a Bruker MultiMode Atomic Force Microscope (AFM) and on a JOEL 1230 High Contrast TEM yielding a size of approximately 3.86 ± 1.27 nm (Fig. 12A, C). Z-potential is also evaluated, and a value of -55.6 ± 13.5 mV is obtained, which lead to the confirmation of the layer of absorbed citrate anions: citrate stabilizes the particles, minimizing aggregation. These anions can be displaced by wet chemistry to fabricate highly ordered arrays[28] self-assembled monolayers,[29] or hybrid lipid bilayers[30].

The BGNP solutions, instead, had a measured Z-potentials of -40.0 ± 6.0 mV. Particles are also observed and measured on a FEI Nova NanoSEM 230 and a JOEL 1230 High Contrast TEM, yielding an average particle diameter of 37.39 ± 5.52 nm (Fig. 12B, D).

Considering both SGNPs and BGNPs, TEM images are used to extract, through the software ImageJ, the dimension of the particles, taking into consideration a statistically relevant number of particles (Fig. 13).

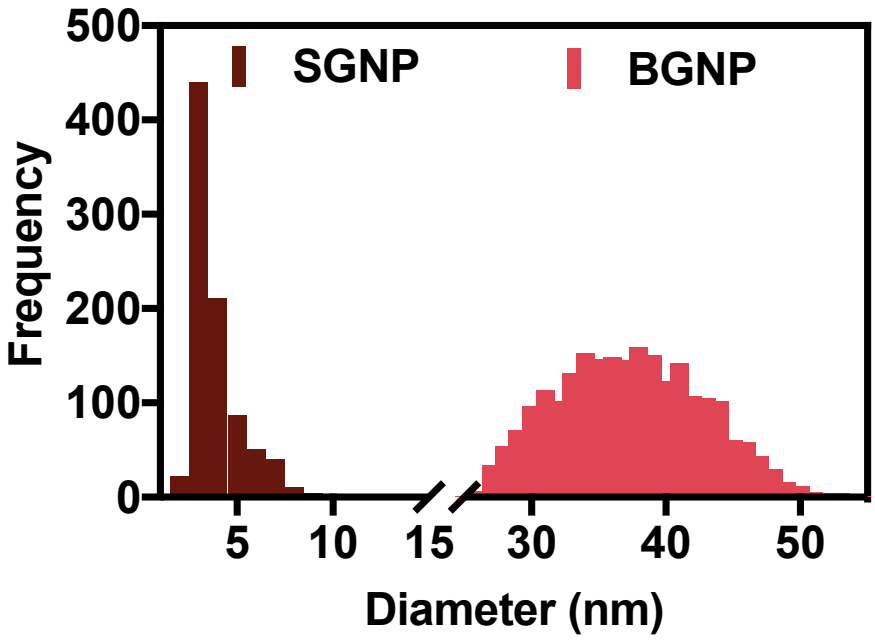

Figure 13. Size distribution of SGNP and BGNP for over 300 particles

Both SGNP and BGNP have a negative value for the Z-potential. The negative z-potential suggests that the colloids are quite stable.

To evaluate the concentration of the samples, using the UV-vis spectrometer, the absorbance spectra are evaluated for both SGNP and BGNP, as reported in Fig. 14.

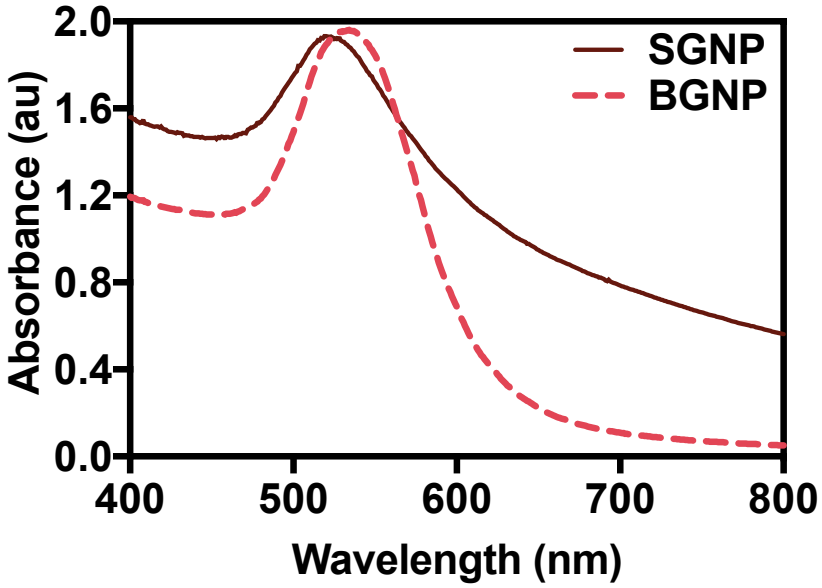

Figure 14. Absorbance spectra of the small (SGNP) and big (BGNP) gold nanoparticles

The maximum absorbance for GNP solutions occurs at 519 nm for SGNP and 534 nm for BGNP. ICP-MS analysis is performed on different samples (as reported in section 4.1.2) to support and compare the theoretical results obtained with MATLAB, starting from UV-vis measurements (section 4.1.1). Table 4 reports all the concentration values.

SAMPLE #	ICP-MS (g/l)	UV-vis (g/l)	Relative error
1	0.1852	0.1236	0.5
2	0.07325	0.0749	0.02
3	4300	3446.4	0.25
4	0.1176	0.1212	0.03
5	0.23905	0.4402	0.45
6	2150	2298	0.06

Table 4. Concentration analysis and comparison

5.2 *In vitro* experiments

5.2.1 Proliferation test on LLC-luciferase expressing cells

As reported in section 4.2.1 IVIS images of LLC-luc cells in a 96 wells plate are acquired, and the ROI are evaluated through software analysis. Imaging is performed immediately prior to eggs and mouse inoculation to verify that the cells maintained their luciferase expression. Figure 15 shows the obtained results.

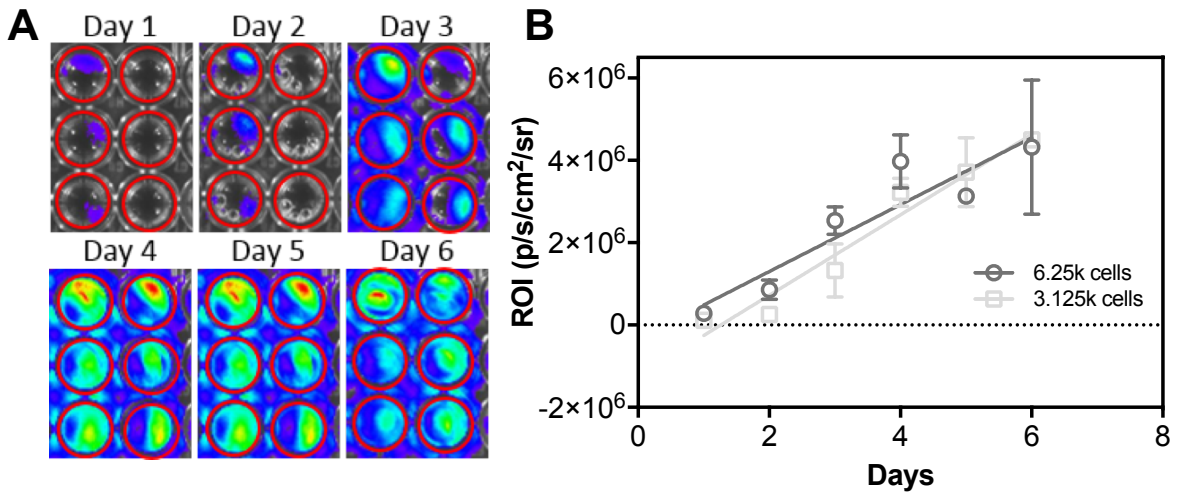

Figure 15. (A) Photo of luciferase expressing LLC-1 cells up to 6 days after seeding. (B) Measured ROI for varying cell number over one week (n=3 wells per group) where a linear fit is applied

Photos of three wells for each concentration are obtained (Fig. 15A), and the measured ROI is plotted over time and fit with a linear regression (Fig. 15B), in which the R^2 values are 0.86 and 0.95 for 6.25K and 3.125K cells, respectively.

Since the experiment was maintained for over one week, low initial seeding densities were required to avoid superconfluence of the cells which would result in cell death.

The results show an increasing trend in luminescence over time. This increase in luminescence with an increasing of the numbers of cells over time, proves that the expression of the luciferase

remains stable also in subsequent generations, making the LLC-luc cell line suitable for in ovo and in vivo experiments.

5.2.2 Cellular uptake *in vitro* study

The size range (shown in section 5.1) allows the GNPs to be internalized via endocytosis into cells without rapid clearance.
Figure 16 A and B shows the internalization of SGNPs and BGNPs, respectively. Reported here are the images corresponding to samples prepared with 54.5 µg of SGNP and 40.85 µg of BGNP. It can be observed that increasing the amount of gold tested with the cells results in a visibly greater amount of gold internalized in the cells.

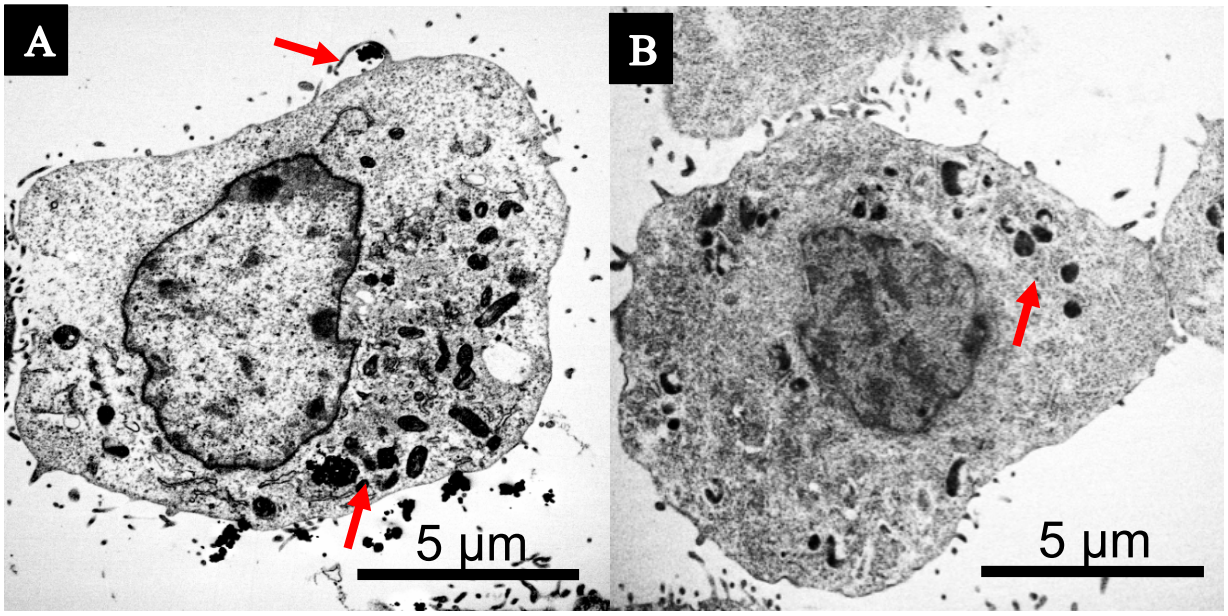

Figure 16. (A) SGNP and (B) BGNP internalized in LLC-luc

The particle clusters remain within vacuoles within the cell. Even without a targeting moiety, macropinocytosis can be visualized in Fig. 16 A (highlighted by red arrows). This is one of four types of endocytosis pathways and is a non-specific process to internalized fluids and particles together into the cells[31]. This observed efficiency in penetrating cells is one of the unique properties of GNP[32] which contributes to their choice of the use, exploited here for radiotherapy.

4.2.3 Comet assay

The Comet assay provides a simple and effective method for evaluating DNA damage in cells and has been widely applied to measure both *in vitro* DNA damage and repair following exposure to various genotoxic agents and for human biomonitoring[33].

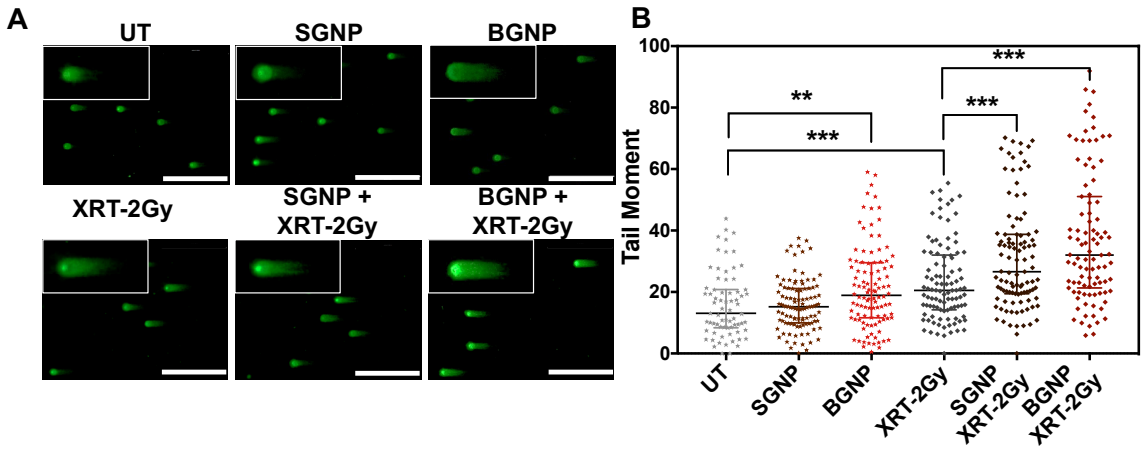

Figure 17. Neutral Comet Assay for LLC1 cells. Cells are untreated (UT), treated with small gold nanoparticles (SGNP) or big gold nanoparticles (BGNP), 2 Gy x-ray irradiation (XRT-2Gy), or a combination of 2 Gy and gold nanoparticles. The horizontal line shows the median and the vertical line shows the interquartile range. At least 50 random cells are scored per sample. An unpaired t-test with Welch's correction is performed to determine statistical significance (**p<0.002 and ***p<0.001).

Figure 17 A shows the visualization of a Neutral Comet Assay by epifluorescence microscopy performed on untreated (UT) LLC-luc cells and cells treated with small gold NP (SGNP) or big gold NP (BGNP), dosed with 2 Gy x-ray irradiation (XRT-2Gy), or irradiated with 2 Gy in the presence of either small or big gold NPs.

The amount of gold incubated with the cells for both the SGNP and BGNP treatment groups is kept constant and is equal to 54.5 µg/well in a 6 well plate with a surface area of 9 cm^2 per well. The same amount of gold is used for the cellular uptake *in vitro* study.

In Fig 17 A it is possible to notice that undamaged DNA remains in the head of the "comet", and the tail represents the amount of damaged DNA (or charged DNA) that migrates in an electric field. A dose of 2 Gy is chosen as it is not only a typical dose used in the literature[3435] but also showed significance in modifying the tail moment when compared to the untreated cells with evidence of a synergistic effect when GNPs are present.

To evaluate the significance of the obtained results, all the data are plotted as a function of the tale moment.

No significance is observed between the UT and SGNP group and some significance (**$p<0.002$) is present between the UT and BGNP groups. Researchers have noticed size dependent toxicity of gold nanoparticles,[36] but it is dependent on assay type, cell line, and nanoparticle properties, leading to conflicting results.

A significant difference is observed (***$p<0.001$) between the UT and XRT-2Gy treatment group and the XRT-2Gy alone and XRT-2Gy with either SGNP and BGNP. It is not surprising that exposure to 2Gy radiation resulted in evidence of a higher tail moment compared to the untreated group, since ionizing radiation is known to produce double-stranded breaks due to the physico-chemical interaction with cellular DNA[33]. However, overall, the greater tail moment for the cells irradiated in the presence of gold nanoparticles indicates that for these two treatment groups, DNA damage is more significant with respect to radiation alone.

5.2.4 Clonogenic assay

Clonogenic assay gives information about the proliferation of LLC-luc cell line. It should be noted that the assay is very sensitive to the attachment grade of the cells on the surface: LLC cells are, by their nature, loosely adherent. This is probably the cause of the low resolution of the image in fig. 18 A. The ability of the cells to replicate decreases significantly after 2 Gy irradiation and 2 Gy irradiation in the presence of both small and big GNPs (Fig. 18).

While the presence of GNPs does not visibly alter the proliferation of the cells into colonies, a reduction in the number of cells can be seen when treated with irradiation alone and combination of GNPs and irradiation (Fig. 18 A).

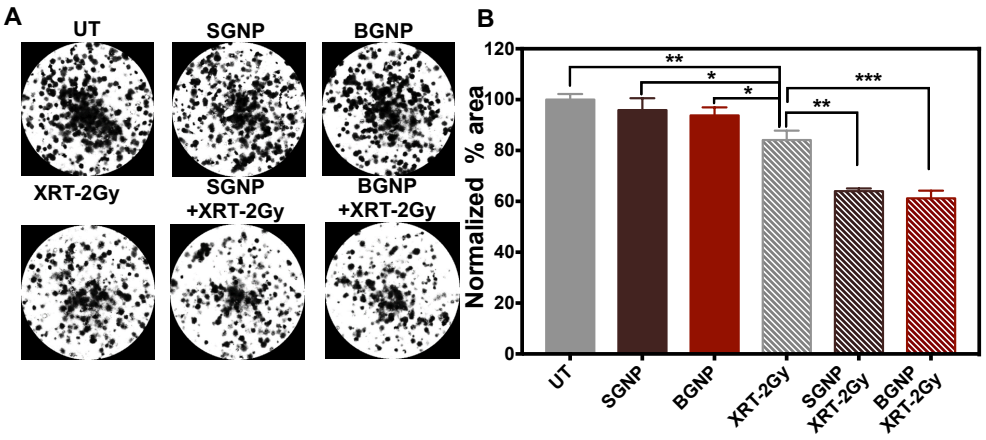

Figure 18. (A) Clonogenic assay performed *in vitro* with LLC1 gives an idea of their capability to form colonies after radiation. (B) Normalized % area for the different treatment groups. Cells from each sample are plated in triplicate. An unpaired t-test with Welch's correction is performed to determine statistical significance (*$p<0.033$, **$p<0.002$, and ***$p\leq0.001$

When the data is represented as a function of the normalized percent area (Fig. 18 B), statistical significance can be evaluated for the different groups.

The three control groups, UT, SGNP, and BGNPs, all show a normalized percent area within error of each other. In the presence of irradiation, however, significance (*$p<0.033$) between the SGNP and XRT-2Gy and BGNP and XRT-2Gy groups is observed, while even greater significance (**$p<0.002$) between the UT and XRT-2Gy can be seen. Moreover, the radiosensitizer effect of the GNPs is indicated by the significance between the XRT-2Gy and SGNP XRT-2Gy groups (**$p<0.002$) and the XRT-2Gy and BGNP XRT-2Gy groups (***$p\leq0.001$). The presence of the particles decreases the % area by 23.9% and 27.2% for the SGNP and BGNP, respectively as compared to the radiation alone (2Gy) group.

While these *in vitro* assays are regarded as accurate methods for measuring and predicting tumor cell radiosensitivity, there are some limitations, whereby for example, excised tumors may fail to grow in soft agar[37] and cells grown as 3D tumors using existing commercial products such as Matrigel use fixed (unchangeable) chemical composition[38] and can survive for only a short period of time without vascular supply. Therefore, there is a vested interest in developing methods for a quicker, more robust, measure of tumor radiosensitivity[37].

5.3 *In ovo* experiments

The chick chorioallantoic membrane (CAM) offers a less common xenograft *in ovo* model to study the effects of GNPs combined with radiotherapy.

The CAM is a membrane that starts to develop in the fecundated chicken egg seven days after fertilization[26] and works as the respiratory system of the chicken embryo. The lack of an immune system and high vascularization result in an ideal environment for tumor growth starting from any kind of tumor cells. Currently, the CAM model is being successfully exploited to the study of drug response of tumors xenografted from patients with the aim to develop personalized therapies according to the needs of each medical case, or to analyze the response to particular drugs, for example, to optimize dose. Other uses include the opportunity to study the vascularization of cancers, angiogenesis, metastasis development[39], and tissue engineering[4041].

Due to the rapid tumor growth, the CAM model was ideally suited for study of the radiosensitivity effects of GNPs. After just four days, three-dimensional tumor growth is observed *in ovo* (Fig. 19). Three-dimensionality is dependent on the number of cells seeded. It has been previously shown that grafting too few cells can result in poor tumor formation (Fig. 19 A), while grafting too many cells can result in either flat sheets with less three-dimensional structure than ideal or tumor overgrowth (Fig. 19 C), in which the tumor occupies the entire silicone ring boundary[26].

Eggs are grafted with $1x10^6$ cells since this number of cells (Fig. 19 B) shows the highest percentage of nice, three-dimensional tumors with a maximum tumor diameter of 3.02 mm ± 0.77, as opposed to the cell sheets observed in the other eggs.

Histology is performed on tumors grown in the CAM for seven days in the presence of GNPs after irradiation. H&E staining (Fig. 20 A) shows the border of a healthy/necrotic region in the tumor demonstrating the effects of a combined treatment of irradiation and GNPs. To visualize the particles within the tissue, dark field imaging after silver stain is performed on a tumor grown in the CAM in the presence of GNPs (Fig. 20 B).

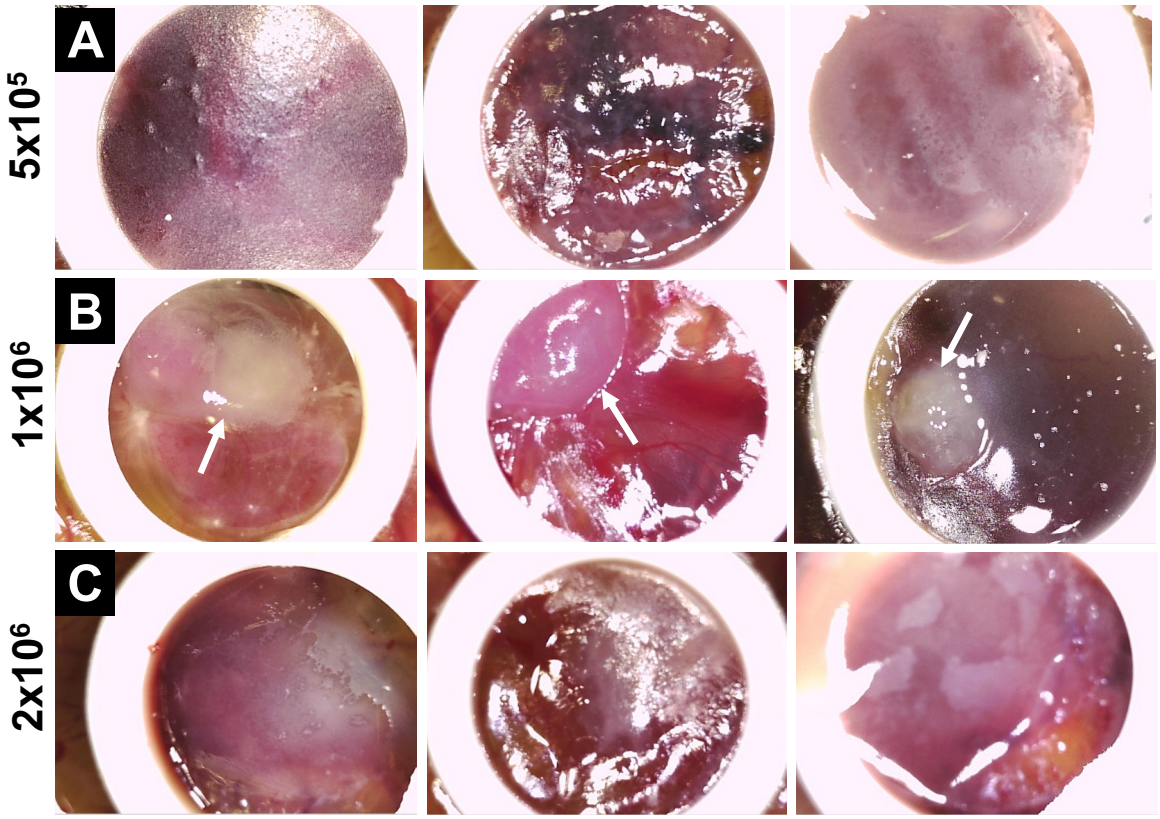

Figure 19. Lewis lung tumor *in ovo* created with (A) $5x10^5$, (B) $1x10^6$, and (C) $2x10^6$ cells. White arrows represent 3D tumor nodules inside the rings.

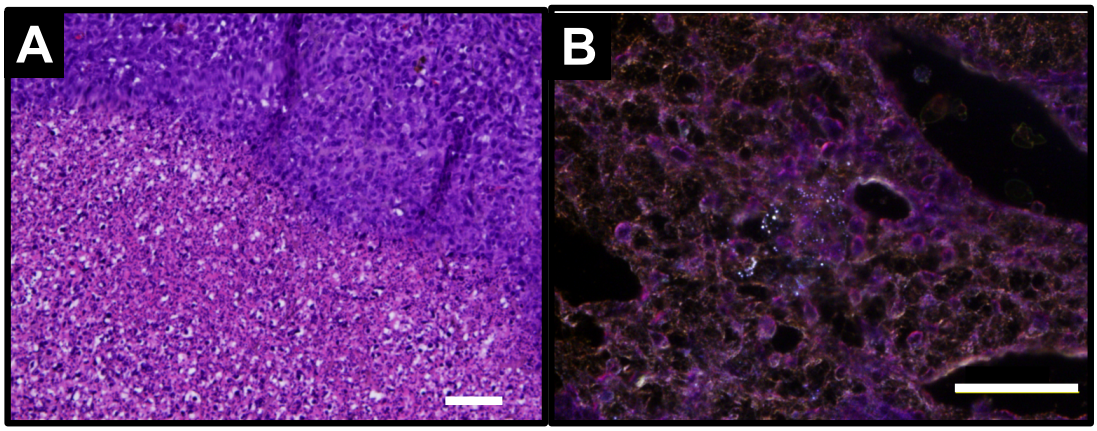

Figure 20. Representative (A) H&E (scale bar is 200 µm) and (B) silver stain (scale bar is 20 µm) from a 3D tumor nodule shown in fig. 20 B

In figure 20 B is possible to notice that the GNPs are perfectly visible, and they appear as silvery points in the images. However, it is hard to distinguish if they are embedded in the tumor or chick tissue, and if they are inside a single cell.

To analyze the silver stained images of a sample the following has to be considered: with optical microscopy with 100x magnification it is only possible to systematically scan the whole slide, losing the overall image.

To further analyze the combined effect of both SGNP and BGNP with radiation, IVIS analysis is performed.

IVIS imaging is used to visualize tumor growth of the luciferase expressing LLC cells within the CAM for the different treatment groups (Fig. 21). Eggs are seeded with cells three days prior to treatment (which occurs on Day 0) and imaged for three days after treatment (Fig. 21) to quantify luminescence intensity and generate a region of interest (ROI).

A dose finding study is first performed to optimize the x-ray irradiation dose within the eggs, whereby it is found that dosing either one or two times with 4 Gy radiation proved too toxic to the eggs. For this reason, a fractionated dose of 2 Gy with one day of recovery in between is chosen.

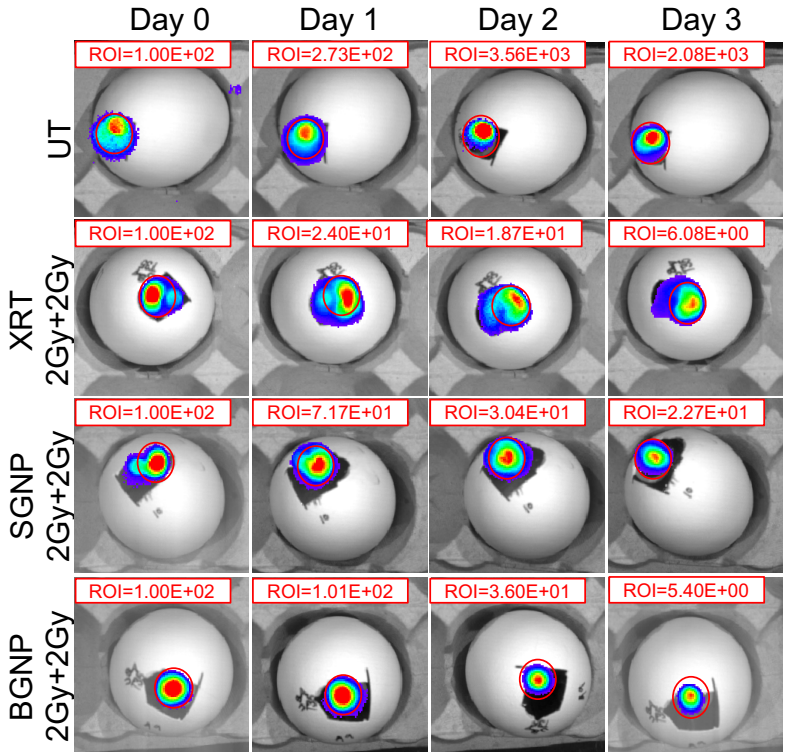

Figure 21. IVIS ROI (p/sec/cm^2/sr) normalized to Day 0 for eggs bearing LLC tumors. Eggs are untreated (UT), treated twice with 2 Gy x-ray irradiation (XRT-2Gy+2Gy), or a combination of 2 Gy + 2 Gy and 7.56 µg of small or big gold nanoparticles

.

To determine the significance in the bioluminescent data over time, ROI values (p/sec/cm^2/sr) are normalized with respect to Day 0 to better assess signal changes (Fig. 22).

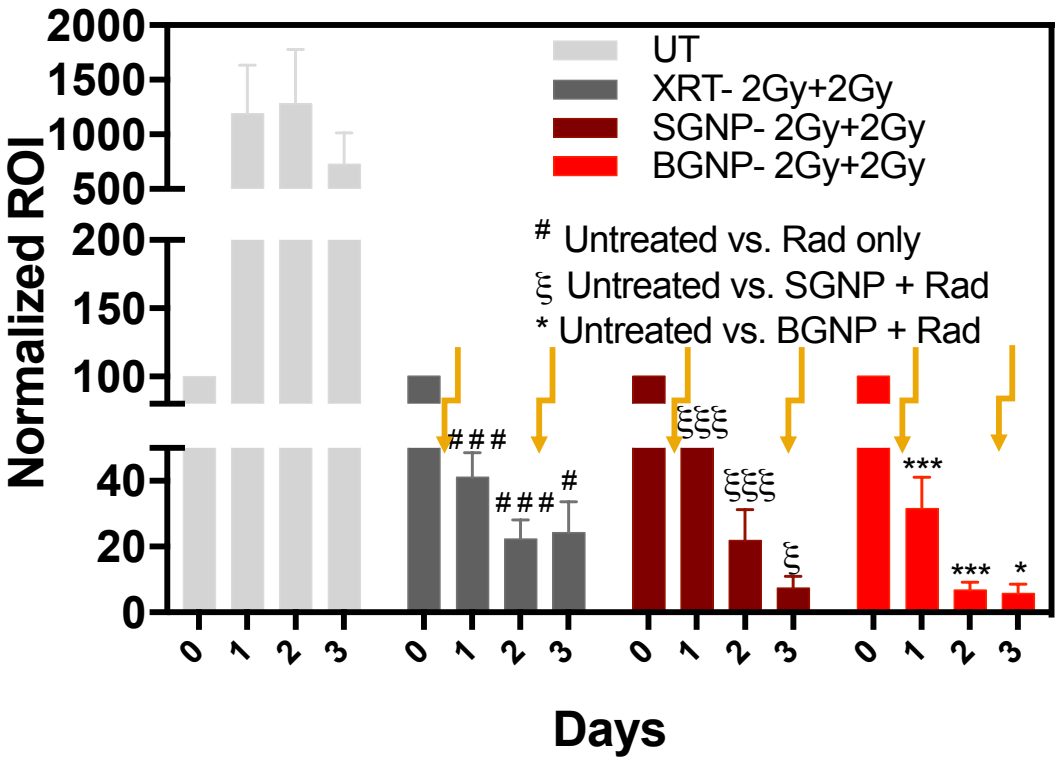

Figure 22. Normalized ROI for the different treatment groups (n=6 per group). 2-way ANOVA was performed to determine statistical significance (*p<0.033, **p<0.002, and ***p<0.001 using New England Journal of Medicine (NEJM) style). Yellow arrow symbols represent radiation treatment

The UT eggs show an increase in signal up to Day 2, (100 on Day 0, 1192 on Day 1, and 1281 on Day 2) which then began to drop on Day 3 (727). The decline in signal on Day 3 maybe attributed to the repeated stress on the eggs with respect to luciferin dosing and removal from the incubator to achieve imaging. Jefferies *et al.*[42] have observed a similar peak and then decline in bioluminescence signal intensity in the CAM with time. Eggs dosed with radiation only or a combined treatment of radiation with small and big GNPs all show a decrease in signal (from 100 to 40, 51, and 31, respectively) after the first dose of 2 Gy on Day 1. After a one-day recovery

period, the signals continue to decline to 22, 22, and 7, respectively, on Day 2. Finally, after a second dose of 2 Gy irradiation the signals become 24, 7, and 6 on Day 3. While a t-test performed for Day 3 does not indicate significance between XRT-2Gy+2Gy and XRT-2Gy+2Gy with GNPs, equality of variance is tested with an F-test, which gave $p=0.02$ (yielding * $p<0.05$) between XRT-2Gy+2Gy and BGNP-XRT-2Gy+2Gy. Further, since a greater signal decline is observed *in ovo* and greater significance observed *in vitro* (Neutral Comet Assay shown in Fig. 2 and Clonogenic assay shown in Fig. 3) with the BGNP treatment group, studies to test the radiosensitizing effect of the GNP progressed to a mouse model.

5.4 *In vivo* experiments

The in vivo experiments are performed on C57/BL6 mice since the cell line is syngeneic to this strain. The choice to proceed with testing only the BGNP was made since a higher decline in signal is observed for the in ovo study using the IVIS with these particles. The decision is also supported by the in vitro results: a greater significance is observed for this size particle for both the Neutral Comet assay (Fig. 17) and Clonogenic assay (Fig. 18).

5.4.1 Preliminary experiments

A preliminary study is made in order to determine the optimal radiation dose for the future experiments on mice to test the efficacy of GNPs as radio sensitizers.

Three irradiation doses, 12, 16, and 20 Gy, are first tested in a mouse model and compared to untreated animals to determine the maximum dose the mice can withstand without detrimental effects as well as the optimal dose to determine GNP enhancement effects (Fig. 23).

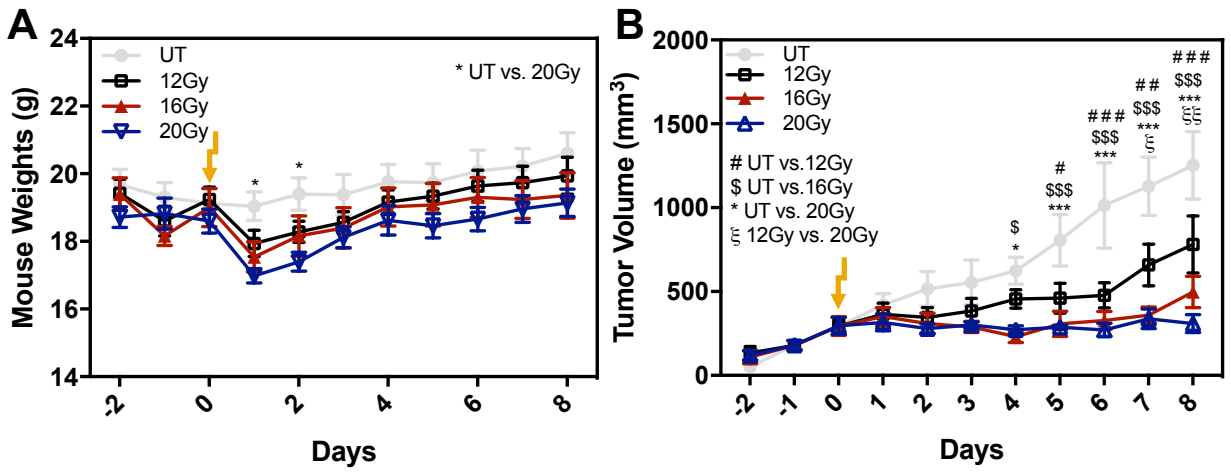

Figure 23. (A) Mouse weights and (B) tumor volumes (n=5) over the course of the study. 2-way ANOVA is performed to determine statistical significance (*p<0.033, **p<0.002, ***p<0.001 using New England Journal of Medicine (NEJM) style). Yellow arrow symbols represent radiation treatment. 5 animals per group.

For all three treatment doses, the mice initially lose weight after irradiation (indicated by the yellow arrow). A significant different in mice weight trend can be noticed on day 2 between the UT and 20 Gy groups, and the mice maintained slightly lower weights until 8 days after treatment (Fig. 23 A).

A dose dependent effect is observed for tumor volume (Fig. 23 B) with 16 Gy and 20 Gy. These two doses display increased significance with time when compared to the UT mice on Days 4, 6, and 8. Instead, the 12 Gy dose shows significance when compared to the UT group beginning on Day 6 (###), however, this dose is not strong enough to maintain such significance as the tumor volume then increased on Day 8 (##). On the last day, Day 8, a significance (!!) between the 12 Gy and 20 Gy doses is determined.

To obtain a complete overview of the different effects of the three doses, necropsy is performed on each mouse, whereby tumor weight and tumor volume are measured (shown in figure 24).

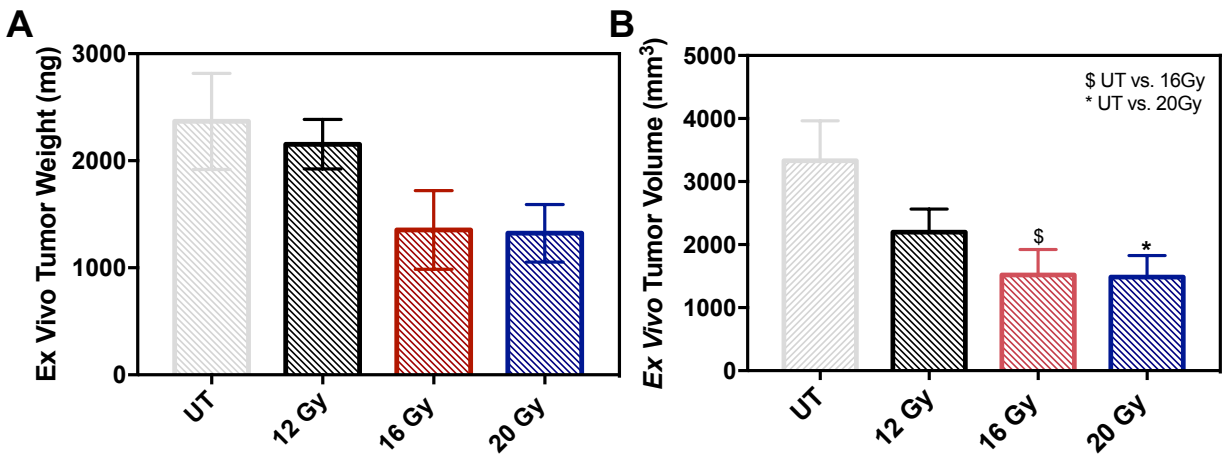

Figure 24. *Ex vivo* tumor (C) weights and (D) volumes (n=5) after eight days. 2-way ANOVA is performed to determine statistical significance (*p<0.033, **p<0.002, ***p<0.001 using New England Journal of Medicine (NEJM) style). 5 animals per group

While there is no significance in *ex vivo* tumor weight on Day 8 (Fig. 24 A), there is significance in tumor volume between the UT group and both the 16 and 20 Gy (Fig. 24 B). Overall, both graphs follow the same trend and the tumors from the 16 and 20 Gy groups show both lower weights and volumes compared to the UT and 12 Gy groups. Therefore, a decision was made to proceed with a dose of 12 Gy to determine if the BGNP can act as effective radiosensitizers because at this dose, the trend in tumor volume can be differentiated from the UT group, and yet it is not too strong of a dose so that tumor growth could then recover over the eight-day experiment.

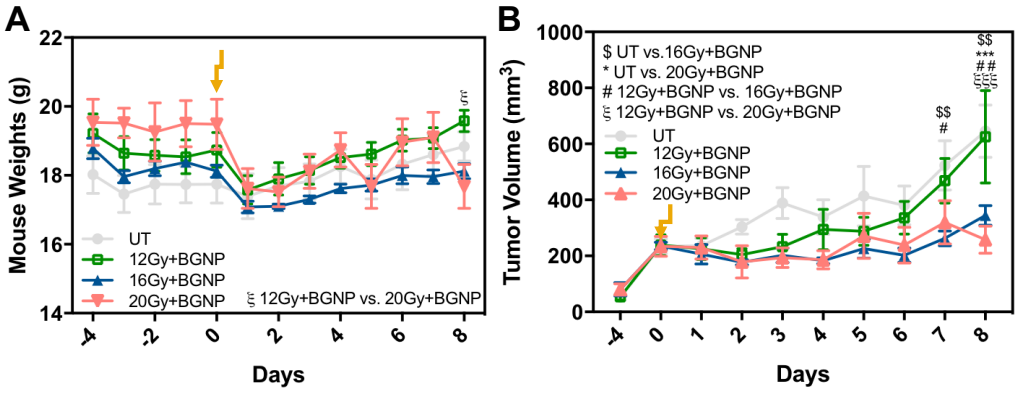

Figure 25. (A) mice weights and (B) tumor volume over time. 2-way ANOVA is performed to determine statistical significance (*p<0.033, **p<0.002, ***p<0.001 using New England Journal of Medicine (NEJM) style). 5 animals per group

The dose founding study is performed with the same groups of animals considering both the effect of three different doses of radiation and the presence of BGNP. The in vivo results over time are shown in Fig. 25.

The mice initially lose weight after irradiation for all the three doses of radiation. Radiation occurs on day 0, as indicated by the yellow arrow. Even if there is a drop in weight on day 2 after treatments, no significance can be determined on Days 2, 4, and 6. On Day 8, there is a significant difference between 12 Gy + BGNP and 20 Gy + BGNP, as shown in Fig. 25 A.

In presence of radiation + BGNP, a dose dependent effect is observed for tumor volume (Fig. 25 B) with 16 Gy and 20 Gy. On Day 7, a significant difference is shown between 12 Gy + BGNP and 16 Gy + BGNP (#), and a greater significance can be seen between UT and 16 Gy + BGNP ($$). More significant results are obtained on Day 8. The same amount of significance is shown between UT and 16 + BGNP and between 12 Gy +BGNP and 16 Gy + BGNP ($$ and ##, respectively). Also, between UT and 20 Gy +BGNP and between 12 Gy + BGNP and 20 Gy + BGNP the significance is the same on Day 8 (*** and ξξξ, respectively).

It is noticeable that the final tumor volumes of Fig. 25 B are drastically lower with respect to the tumor volumes displayed in Fig. 23 B, in which the effect of the radiation alone is exploited.

To obtain a complete overview on the different effect of the three doses in the presence of BGNP, necropsy is performed on each mouse, whereby tumor weight and tumor volume are measured.

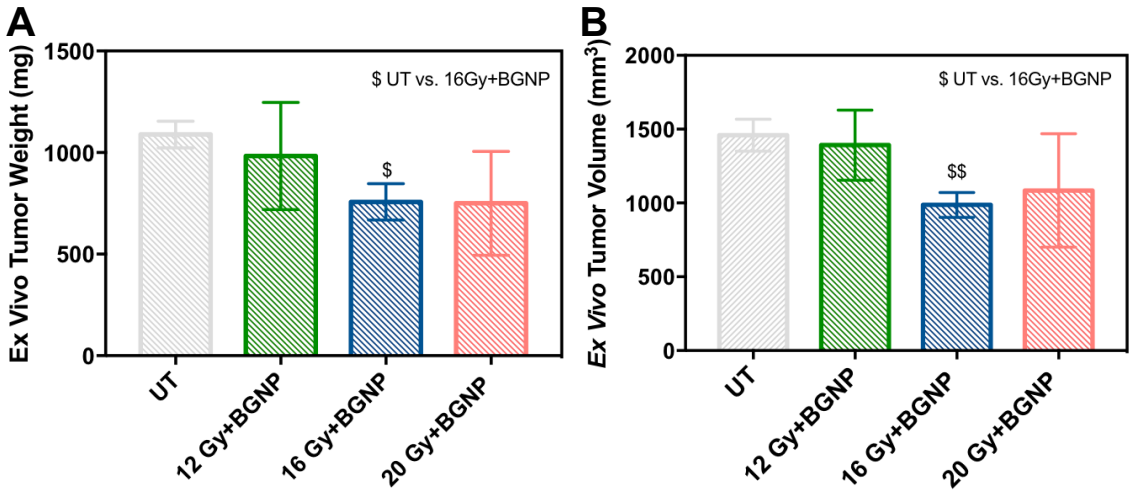

Figure 26. *Ex vivo* tumor (C) weights and (D) volumes (n=5) after eight days. 2-way ANOVA is performed to determine statistical significance (*p<0.033, **p<0.002, ***p<0.001 using New England Journal of Medicine (NEJM) style). 5 animals per group

A significance in *ex vivo* tumor weight on Day 8 (Fig. 26 A) is exhibited between UT and 16 Gy + BGNP ($). A greater significance can be measured between the same groups considering the *ex vivo* tumor volume ($$), as shown in Fig. 28 B.
A comparison between the *ex vivo* tumor volumes with and without BGNP (Fig.26 B and Fig. 24 B, respectively) shows, as in the case of the tumor volumes over time, that the tumor volumes are smaller after eight days when the effect of BGNP is involved in the treatments.
It is possible to visualize the BGNP inside the mice tumor tissue by analyzing histological samples with silver stained. Images are taken with a dark field microscope, as reported in section 3.5.

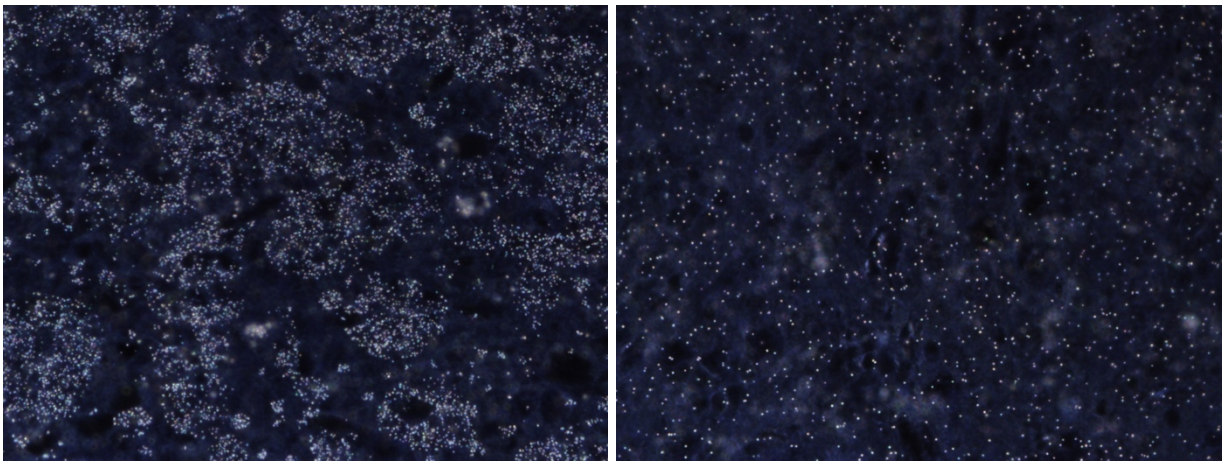

Figure 27. Two different sections of histological sample, silver stained, of mouse tumor tissue

Comparing Fig. 27 with Fig. 20 B, the difference between the amount of gold inoculated into the eggs versus that injected into the mice tumor is clearly observable. The number of bright spots is directedly correlated to the number of BGNP in the tumor tissue. The egg sample, shown in Fig. 20 B, shows few bright spots, which corresponds to a dose of 7.56 μg of gold inoculated in the entire tumor volume. In the mouse sample (Fig. 27), the number of bright spots is increased, and the amount of gold injected into the tumor, prior irradiation, is 0.215 mg. The results obtained with this second preliminary experiment support the efficacy of using BGNP to enhance the effect of radiation. To demonstrate this hypothesis the decision to proceed with a irradiation dose of 12 Gy is made, as mentioned above, due to the effect of this dose on mice: the trend of tumor volume of 12 Gy group can be differentiated from the UT, but the efficacy of the radiation is not strong enough to completely suppress the ion enhancing effects of the BGNP.

5.4.2 Mice experiments

In order to evaluate the response of the mice and to verify that the animal can physically support the treatment, different vital parameters are measured, including mice weights and internal body temperature.

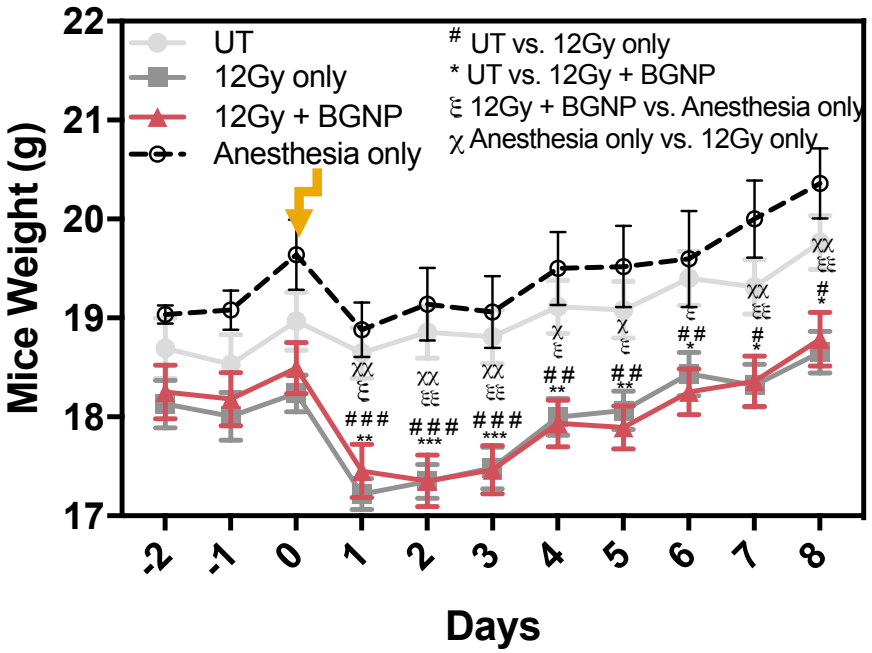

Figure 28. Mouse weights for various treatment groups (n=15 per group, arrows represent irradiation time points). To determine statistical significance 2-way ANOVA was performed (*p<0.033, **p<0.002, and ***p<0.001 using New England Journal of Medicine (NEJM) style)

Figure 28 shows the mouse weights over the course of the experiment, where irradiation occurs on Day 0 (signified by the arrow). The average weight of the untreated group remains stable over 8 days while the average weights of the 12 Gy only and 12 Gy + BGNP groups drop the day after treatment. An additional group (n=5) is shown in Fig.28 to compare the effects of anesthesia alone (solid grey trace, closed circles) with the combined effects of anesthesia and irradiation (dashed black trace, open circles). Although not statistically significant, it can be seen that the use of an injectable anesthesia (Dexdomitor) in addition to an inhalant (isoflurane) in the absence of irradiation causes a reduction in body weight.

Dexomitor is known to cause depression of gastrointestinal motility due to decrease in smooth muscle activity[43]. However, these animals recover more rapidly than those that are also exposed to 12 Gy irradiation. At this dose the irradiation may damage the gastrointestinal system in the mice resulting in the observed weight loss[44]. Since the statistical significance between untreated and 12Gy irradiation and untreated and 12 Gy irradiation + BGNP are similar across the treatment period, it should be concluded that the presence of the nanoparticles themselves do not affect changes in body weight.

It should be noted that no other changes in physiology indicative of illness in the mice are observed also analyzing the body temperature, shown in Fig. 29.

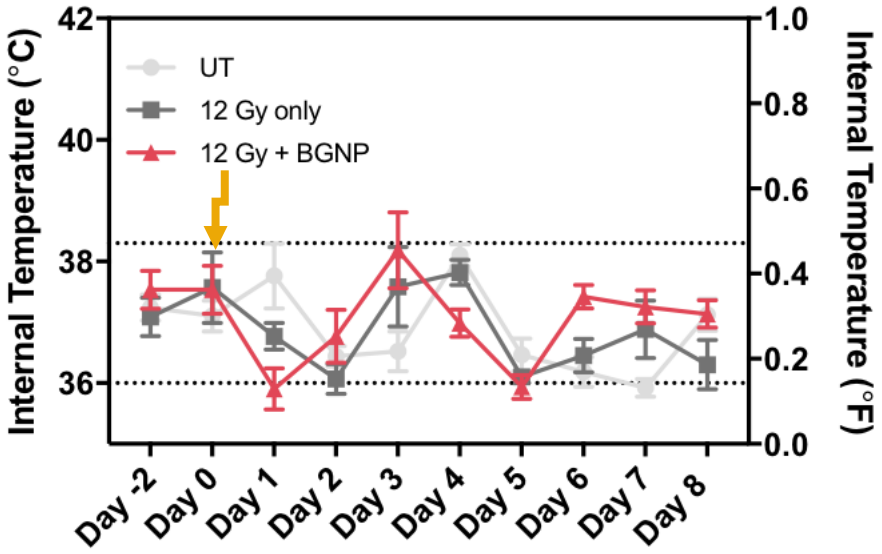

Figure 29. Mouse body temperature for various treatment groups (n=10 per group, arrows represent irradiation time points, dashed horizontal lines represent the normal range for internal body temperature)

The dashed lines represented in Fig. 29 symbolize the range in which the mouse temperature can be considered normal. Over the time during which the mice are monitored, all of the groups show an average body temperature within this range. According to the fluctuant trend of this parameter for all the groups, is possible to assert that there is no correlation between the treatment type and body temperature.

These two results allow for the conclusion that mice can withstand both the treatments (radiation alone and radiation in combination with BGNP) without showing signs of illness.

By measuring tumor volumes every day, the efficacy in controlling tumor growth according to the treatment type it is proven. Results are shown in Fig. 30.

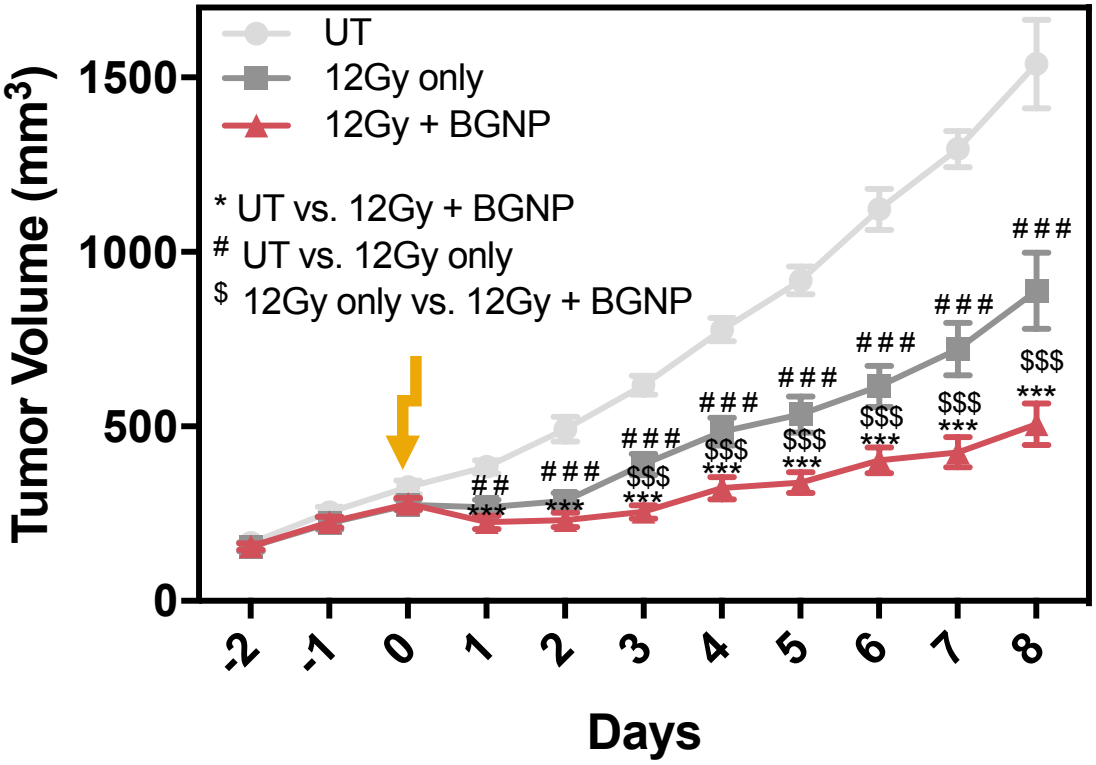

Figure 30. Tumor volume for various treatment groups (n=15 per group, arrows represent irradiation time points). To determine statistical significance 2-way ANOVA was performed (*p<0.033, **p<0.002, and ***p<0.001 using New England Journal of Medicine (NEJM) style

The experiment last 8 days because the primary tumor volumes in the untreated mice approach the IACUC euthanasia criteria outlined in the animal protocol and if left uncontrolled would interfere with normal physiological function of the mouse.

Prior to treatment (indicated by the arrow on Day 0), tumor growth rate is the same for all groups. Post treatment, mice administered with BGNPs intratumorally and dosed with 12 Gy radiation have significantly smaller tumor volumes with respect to the untreated mice, which increase exponentially. Starting from day 3, a significant difference is also evident between the radiation only group and BGNP + radiation group. These results indicate the efficacy of treatment with BGNPs, even with just one injection and irradiation occurrence.

IVIS analysis is also performed to evaluate the bioluminescence response of the tumors in mice over time.

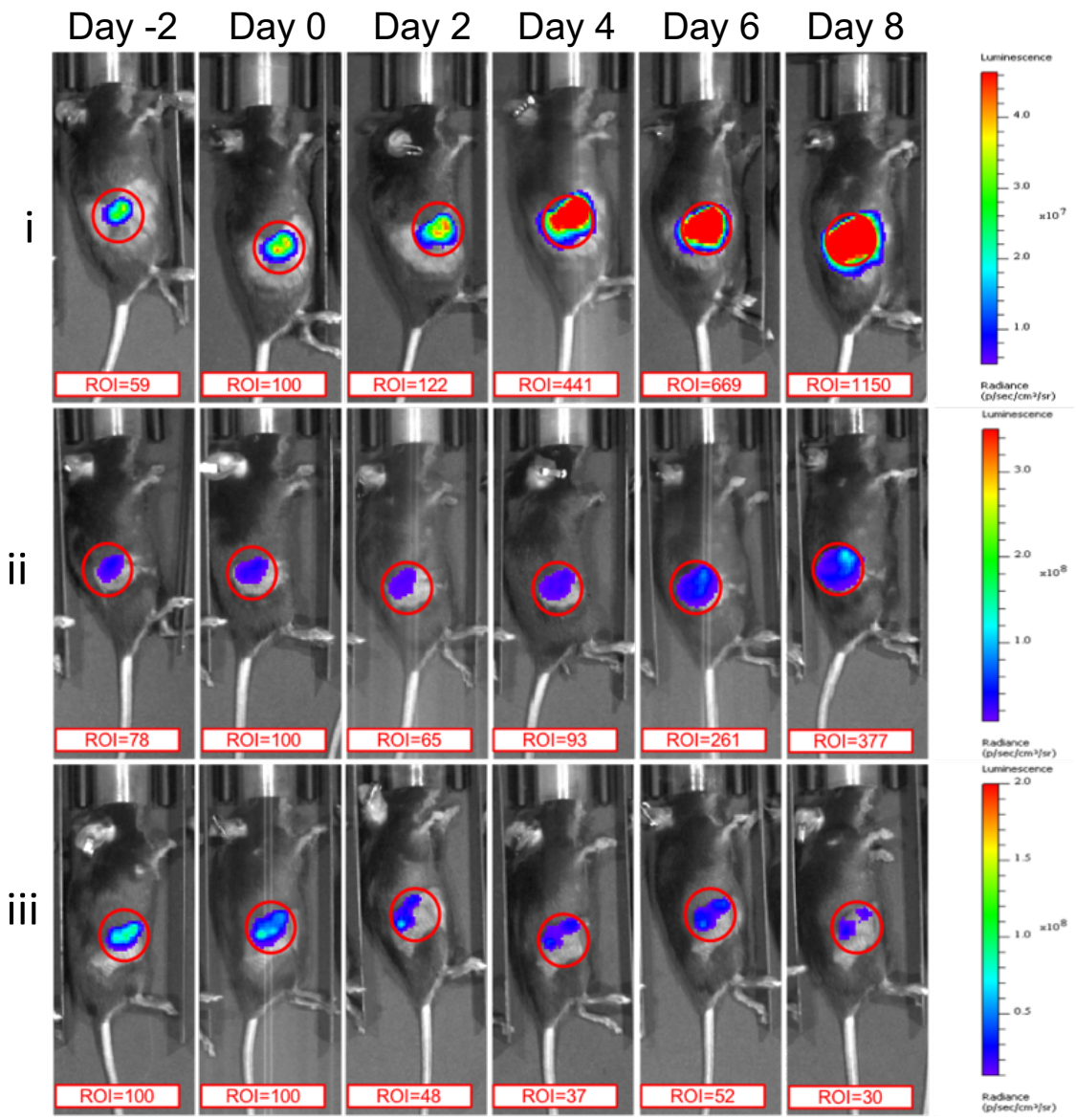

Figure 31. IVIS images for representative mice with LLC-1 tumors. Mice are (i) untreated (UT), (ii) treated once with 12 Gy x-ray radiation, and (iii) treated once with 12 Gy x-ray + BGNP

Five mice (each group is composed by 15 mice in total) can be imaged together. In Fig. 31 one representative mouse per group is shown over time, and the ROI values over time are included for each mouse. Setting the same scale bar over time for the single mouse is possible, by eye, to see the increase of the luminescence signal for the untreated group and the decrease of signal for the groups treated with radiation alone and radiation + BGNP. To have an overall trend for all the mice

which compose the three groups, the average ROI value for each group, normalized with respect to Day 0, is reported in Fig. 32.

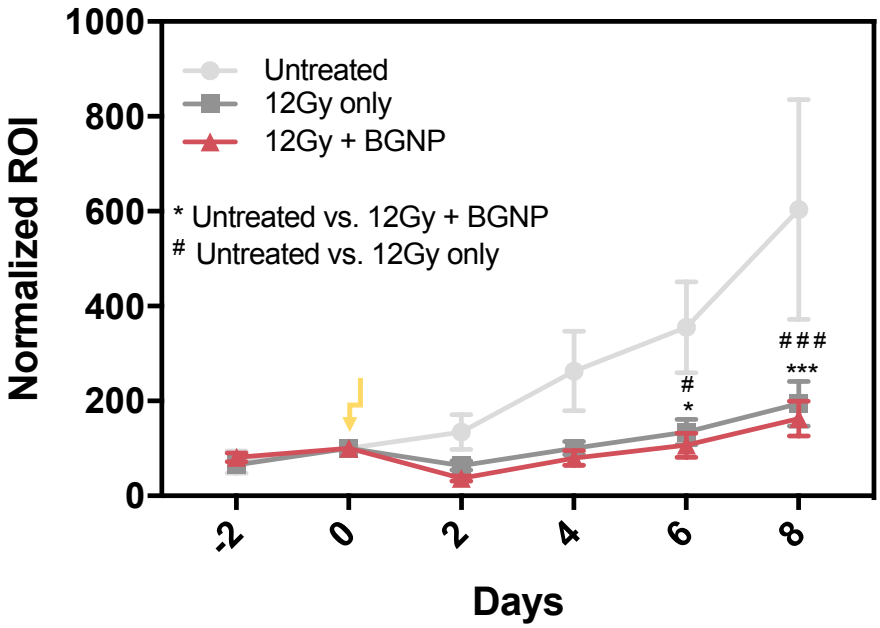

Figure 32. Normalized luminescence intensity of ROI (n=15 per group, arrows represent irradiation time points). 2-way ANOVA is performed to determine statistical significance (*p<0.033, **p<0.002, and ***p<0.001 using New England Journal of Medicine (NEJM) style)

The irradiation and the BGNP injection occur on Day 0, and even if the untreated group has an extremely different behavior over time with respect the other groups, it is not possible to observe a significant difference between the signal of radiation alone group and radiation + BGNP group; both of them show the same increase of significance if compared with the UT group over time. There are several possible explanations for this result. First of all, a large number of mice had tumors that were exposed, which means that the tumors appeared ulcerated, such that the tumor tissue is exposed. Signal that comes from a more superficial source is higher, and this can lead to the minimal difference between the 12 Gy only and the 12 Gy + BGNP. Another possible cause of this result can be the location of the tumor. LLC-luc cells are inoculated in the right flank of the anesthetized mice, subcutaneously, but, even if the procedure is followed carefully, not all of the cells are inoculate at the same depth under the skin and this causes the growth of tumors in different positions and profundities, leading to inhomogeneous signals within the same treatment group. In

order to assess the intratumoral delivery and localization of the BGNP in vivo CT imaging is performed on the mice.

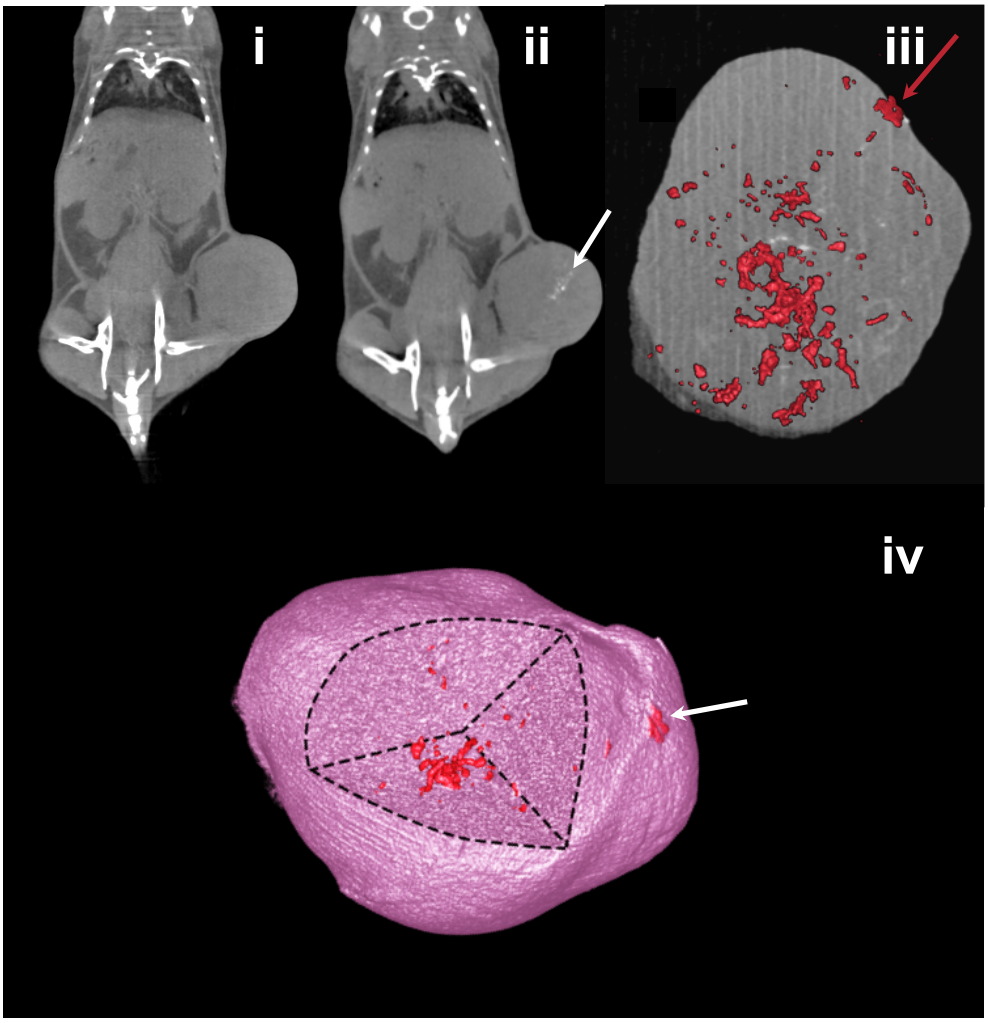

Figure 33. In vivo microCT scan of a tumor bearing mouse (i) before and (ii) after BGNP injection shown with 105 mm resolution and ex vivo tumor (iii) slice superimposed with 3D rendering of BGNPs and (iv) 3D rendering of the entire tumor where a section has been made transparent to show BGNP location shown with 40 mm resolution (arrows represent injection entry site)

Figure 33 represents a tumor bearing mouse located on the flank pre- (Fig. 32 i) and post- (Fig. 33 ii) intratumoral injection of BGNPs imaged from a coronal view. The presence of BGNPs increases the contrast difference within the tissue and allows for their localization. Immediately, post-

injection the particles are well distributed within the entire tumor volume (Fig. 33 iii) and the injection site can be identified by the linear path of particles left behind (red arrow).
It is possible to assert that even after seven days, re-imaging the tumor site shows similar particle distribution and density. A 3D rendering of the tumor with a section view cut out (Fig. 33 iv) highlights an area within the tumor with high particle density allowing for increased contrast.

Chapter 6

Conclusions and future work

This thesis examines the effectiveness of two different dimensions of GNP, synthetized in the lab, as radiosensitizers in vitro, in ovo, and in vivo in a mouse model of lung cancer.

Comet and clonogenic assays demonstrate that in the presence of 2 Gy X-ray irradiation, both particle sizes present larger tail moments and decreased colony area when compared to no treatment and irradiation alone.

In ovo system, employing the CAM assay, offers a method for non-invasive, live imaging of the tumor model and allows for the study of the effects of radiation and GNP treatment. Through topical application of luciferin in the egg and IVIS imaging, an increase in luminescence signal is observed in untreated eggs, whereas eggs dosed with radiation only or a combined treatment of radiation with small and big GNPs all showed declining signals. These results support the further development of bioluminescent CAM assays for assessment of irradiation and combined radiative treatments.

In vivo CT imaging allows for localization of the BGNPs in mice, which still remained visible seven days after intratumoral injection. A significant difference in tumor volume between untreated mice and mice treated with radiation alone is shown over time, and also a significant differentiation in tumor growth is manifested between mice treated with radiation alone and mice treated with the combined effect of radiation and BGNPs.

Therefore, this work successfully demonstrates the radiosensitization of gold NP in vitro and in two different animal models.

Future directions include the creation of a survival curve for the mouse model, to understand the different behaviors of radiation alone, treated mice, and mice treated with the combination of 12 Gy and BGNP several weeks after treatment.

The use of CT imaging can be also used to validate the manual measurements of tumor volume in mice over time: through the use of the CT software, it is possible to accurately measure the two principal dimensions of the 3D reconstructed mouse tumor and compare these measurements with the ones obtained from measuring the tumor with a caliper. Computer Tomography can also be used to investigate the difference in distribution of GNPs according to the injection site, demonstrating that intratumoral injection is the best approach to avoid dispersion of GNPs in unwanted areas.

This technique can ultimately be employed to visualize both the tumor itself and tumor growth in eggs in order to compare the tumor volumes between treatment groups at the end of the experiment. This procedure is difficult to manually perform due to the small dimension of the tumor in the egg and the difficulty to distinguish by eye the tumor tissue from the chicken one.

Another possible direction to exploit is the functionalization of GNPs, for example with conjugated antibody, to enhance not only the radiation effect but also the immune response.

Bibliography

(1) Siegel, R. L.; Miller, K. D.; Jemal, A. Cancer Statistics, 2018. *Cancer Stat. 2018*.

(2) Mariotto, A. B.; Robin Yabroff, K.; Shao, Y.; Feuer, E. J.; Brown, M. L. Projections of the Cost of Cancer Care in the United States: 2010-2020. *JNCI J. Natl. Cancer Inst.* **2011**, *103* (2), 117–128.

(3) Baskar, R.; Lee, K. A.; Yeo, R.; Yeoh, K.-W. Cancer and Radiation Therapy: Current Advances and Future Directions. *Int. J. Med. Sci.* **2012**, *9* (3), 193–199.

(4) Delaney, G.; Jacob, S.; Featherstone, C.; Barton, M. The Role of Radiotherapy in Cancer Treatment: Estimating Optimal Utilization from a Review of Evidence-Based Clinical Guidelines. *Cancer* **2005**, *104* (6), 1129–1137.

(5) Jackson, S. P.; Bartek, J. The DNA-Damage Response in Human Biology and Disease. *Nature* **2009**, *461* (7267), 1071–1078.

(6) Butterworth, K. T.; McMahon, S. J.; Currell, F. J.; Prise, K. M. Physical Basis and Biological Mechanisms of Gold Nanoparticle Radiosensitization. *Nanoscale* **2012**, *4* (16), 4830.

(7) Jaffray, D. A. Image-Guided Radiotherapy: From Current Concept to Future Perspectives. *Nat. Rev. Clin. Oncol.* **2012**, *9* (12), 688–699.

(8) Begg, A. C.; Stewart, F. A.; Vens, C. Strategies to Improve Radiotherapy with Targeted Drugs. *Nat. Rev. Cancer* **2011**, *11* (4), 239–253.

(9) Engineered Nanoparticles in Cancer Therapy.

(10) Her S1, Jaffray DA2, Allen C3. Gold Nanoparticles for Applications in Cancer Radiotherapy: Mechanisms and Recent Advancements.

(11) Arvizo, R.; Bhattacharya, R.; Mukherjee, P. Gold Nanoparticles: Opportunities and Challenges in Nanomedicine. *Expert Opin. Drug Deliv.* **2010**, *7* (6), 753–763.

(12) Popovtzer, R.; Agrawal, A.; Kotov, N. A.; Popovtzer, A.; Balter, J.; Carey, T. E.; Kopelman, R. Targeted Gold Nanoparticles Enable Molecular CT Imaging of Cancer. *Nano Lett.* **2008**, *8* (12), 4593–4596.

(13) Huang, X.; El-Sayed, I. H.; Qian, W.; El-Sayed, M. A. Cancer Cell Imaging and Photothermal Therapy in the Near-Infrared Region by Using Gold Nanorods. *J. Am. Chem. Soc.*

2006, *128* (6), 2115–2120.

(14) Zheng, Y.; Cloutier, P.; Hunting, D. J.; Sanche, L. Radiosensitization by Gold Nanoparticles: Comparison of DNA Damage Induced by Low and High-Energy Electrons. *J. Biomed. Nanotechnol.* **2008**, *4* (4), 469–473.

(15) Pan, Y.; Leifert, A.; Ruau, D.; Neuss, S.; Bornemann, J.; Schmid, G.; Brandau, W.; Simon, U.; Jahnen-Dechent, W. Gold Nanoparticles of Diameter 1.4 Nm Trigger Necrosis by Oxidative Stress and Mitochondrial Damage. *Small* **2009**, *5* (18), 2067–2076.

(16) Lin, W.; Huang, Y.; Zhou, X.-D.; Ma, Y. In Vitro Toxicity of Silica Nanoparticles in Human Lung Cancer Cells. *Toxicol. Appl. Pharmacol.* **2006**, *217* (3), 252–259.

(17) Mackey, M. A.; El-Sayed, M. A. Chemosensitization of Cancer Cells *via* Gold Nanoparticle-Induced Cell Cycle Regulation. *Photochem. Photobiol.* **2014**, *90* (2), 306–312.

(18) Duff, D. G.; Baiker, A.; Edwards, P. P. A New Hydrosol of Gold Clusters. 1. Formation and Particle Size Variation. *Langmuir* **1993**, *9* (9), 2301–2309.

(19) Jalili, N.; Laxminarayana, K. A Review of Atomic Force Microscopy Imaging Systems: Application to Molecular Metrology and Biological Sciences. *Mechatronics* **2004**, *14* (8), 907–945.

(20) Bhattacharjee, S. DLS and Zeta Potential – What They Are and What They Are Not? *J. Controlled Release* **2016**, *235*, 337–351.

(21) Khlebtsov, N. G. Determination of Size and Concentration of Gold Nanoparticles from Extinction Spectra. *Anal. Chem.* **2008**, *80* (17), 6620–6625.

(22) Campeau, E.; Ruhl, V. E.; Rodier, F.; Smith, C. L.; Rahmberg, B. L.; Fuss, J. O.; Campisi, J.; Yaswen, P.; Cooper, P. K.; Kaufman, P. D. A Versatile Viral System for Expression and Depletion of Proteins in Mammalian Cells. *PLoS ONE* **2009**, *4* (8), e6529.

(23) Hastings, J. W. Chemistries and Colors of Bioluminescent Reactions: A Review. *Gene* **1996**, *173* (1 Spec No), 5–11.

(24) Gyori, B. M.; Venkatachalam, G.; Thiagarajan, P. S.; Hsu, D.; Clement, M.-V. OpenComet: An Automated Tool for Comet Assay Image Analysis. *Redox Biol.* **2014**, *2*, 457–465.

(25) Franken, N. A. P.; Rodermond, H. M.; Stap, J.; Haveman, J.; van Bree, C. Clonogenic

Assay of Cells in Vitro. *Nat. Protoc.* **2006**, *1* (5), 2315–2319.
(26) Li, M.; Pathak, R. R.; Lopez-Rivera, E.; Friedman, S. L.; Aguirre-Ghiso, J. A.; Sikora, A. G. The In Ovo Chick Chorioallantoic Membrane (CAM) Assay as an Efficient Xenograft Model of Hepatocellular Carcinoma. *J. Vis. Exp.* **2015**, No. 104.
(27) Uchihara, T. Silver Diagnosis in Neuropathology: Principles, Practice and Revised Interpretation. *Acta Neuropathol. (Berl.)* **2007**, *113* (5), 483–499.
(28) Wang, H.; Levin, C. S.; Halas, N. J. Nanosphere Arrays with Controlled Sub-10-Nm Gaps as Surface-Enhanced Raman Spectroscopy Substrates. *J. Am. Chem. Soc.* **2005**, *127* (43), 14992–14993.
(29) Levin, C. S.; Janesko, B. G.; Bardhan, R.; Scuseria, G. E.; Hartgerink, J. D.; Halas, N. J. Chain-Length-Dependent Vibrational Resonances in Alkanethiol Self-Assembled Monolayers Observed on Plasmonic Nanoparticle Substrates. *Nano Lett.* **2006**, *6* (11), 2617–2621.
(30) Levin, C. S.; Kundu, J.; Janesko, B. G.; Scuseria, G. E.; Raphael, R. M.; Halas, N. J. Interactions of Ibuprofen with Hybrid Lipid Bilayers Probed by Complementary Surface-Enhanced Vibrational Spectroscopies. *J. Phys. Chem. B* **2008**, *112* (45), 14168–14175.
(31) Park, J. H.; Oh, N. Endocytosis and Exocytosis of Nanoparticles in Mammalian Cells. *Int. J. Nanomedicine* **2014**, 51.
(32) Xie, X.; Liao, J.; Shao, X.; Li, Q.; Lin, Y. The Effect of Shape on Cellular Uptake of Gold Nanoparticles in the Forms of Stars, Rods, and Triangles. *Sci. Rep.* **2017**, *7* (1).
(33) Garaj-Vrhovac, V.; Kopjar, N. The Alkaline Comet Assay as Biomarker in Assessment of DNA Damage in Medical Personnel Occupationally Exposed to Ionizing Radiation. *Mutagenesis* **2003**, *18* (3), 265–271.
(34) Kurashige, T.; Shimamura, M.; Nagayama, Y. Differences in Quantification of DNA Double-Strand Breaks Assessed by 53BP1/ΓH2AX Focus Formation Assays and the Comet Assay in Mammalian Cells Treated with Irradiation and N-Acetyl-L-Cysteine. *J. Radiat. Res. (Tokyo)* **2016**, *57* (3), 312–317.
(35) Dunne, A. L.; Price, M. E.; Mothersill, C.; McKeown, S. R.; Robson, T.; Hirst, D. G. Relationship between Clonogenic Radiosensitivity, Radiation-Induced Apoptosis and DNA Damage/Repair in Human Colon Cancer Cells. *Br. J. Cancer* **2003**, *89*, 2277.

(36) Alkilany, A. M.; Murphy, C. J. Toxicity and Cellular Uptake of Gold Nanoparticles: What We Have Learned so Far? *J. Nanoparticle Res.* **2010**, *12* (7), 2313–2333.
(37) McKenna, D. J.; McKeown, S. R.; McKelvey-Martin, V. J. Potential Use of the Comet Assay in the Clinical Management of Cancer. *Mutagenesis* **2008**, *23* (3), 183–190.
(38) Souza, G. R.; Molina, J. R.; Raphael, R. M.; Ozawa, M. G.; Stark, D. J.; Levin, C. S.; Bronk, L. F.; Ananta, J. S.; Mandelin, J.; Georgescu, M.-M.; et al. Three-Dimensional Tissue Culture Based on Magnetic Cell Levitation. *Nat. Nanotechnol.* **2010**, *5* (4), 291–296.
(39) Deryugina, E. I.; Quigley, J. P. Chick Embryo Chorioallantoic Membrane Model Systems to Study and Visualize Human Tumor Cell Metastasis. *Histochem. Cell Biol.* **2008**, *130* (6), 1119–1130.
(40) Moreno-Jiménez, I.; Hulsart-Billstrom, G.; Lanham, S. A.; Janeczek, A. A.; Kontouli, N.; Kanczler, J. M.; Evans, N. D.; Oreffo, R. O. The Chorioallantoic Membrane (CAM) Assay for the Study of Human Bone Regeneration: A Refinement Animal Model for Tissue Engineering. *Sci. Rep.* **2016**, *6* (1).
(41) Farina, M.; Chua, C. Y. X.; Ballerini, A.; Thekkedath, U.; Alexander, J. F.; Rhudy, J. R.; Torchio, G.; Fraga, D.; Pathak, R. R.; Villanueva, M.; et al. Transcutaneously Refillable, 3D-Printed Biopolymeric Encapsulation System for the Transplantation of Endocrine Cells. *Biomaterials* **2018**, *177*, 125–138.
(42) Jefferies, B.; Lenze, F.; Sathe, A.; Truong, N.; Anton, M.; von Eisenhart-Rothe, R.; Nawroth, R.; Mayer-Kuckuk, P. Non-Invasive Imaging of Engineered Human Tumors in the Living Chicken Embryo. *Sci. Rep.* **2017**, *7* (1).
(43) package insert Dexdomitor https://www.zoetisus.com/_locale-assets/mcm-portal-assets/products/pdf/cad_pis/dexdomitor_pi.pdf (accessed May 19, 2018).
(44) Booth, C.; Tudor, G.; Tudor, J.; Katz, B. P.; MacVittie, T. J. Acute Gastrointestinal Syndrome in High-Dose Irradiated Mice. *Health Phys.* **2012**, *103* (4), 383–399.